August 2020

Exploiting the Asymmetric Energy Barrier in Multi-Stable Origami to Enable Mechanical Diode Behavior

Nasim Baharisangari
Clemson University, nbaharisangari@gmail.com

Exploiting the Asymmetric Energy Barrier in Multi-stable Origami to Enable Mechanical Diode Behavior

A Thesis
Presented to
the Graduate School of
Clemson University

In Partial Fulfillment
of the Requirements for the Degree
Master of Science
Mechanical Engineering

by
Nasim Baharisangari
August 2020

Accepted by:
Dr. Suyi Li, Committee Chair
Dr. Oliver Myers
Dr. Lonny Thompson

Abstract

Recently, multi-stable origami have drawn many attentions for their potential applications in multi-functional structures and material systems. Especially, origami folding is essentially a three-dimensional mechanism, which induces unorthodox properties that distinguish this mechanism from its traditional counterparts. This study proposes a multi-stable origami cellular structure that can exhibit mechanical diode behavior in compression. Furthermore, with a small variation in the unit cell of the proposed structure, a extension diode can be achieved. Such structures consist of many stacked Miura-ori sheets, and can be divided into unit cells that pose two different stable configurations. To understand and elucidate the underlying mechanisms, two adjacent unit cells were considered as the most fundamental constituents of the cellular structures that display the desired diode behavior. This study examines how folding can impose a kinematic constraint onto the deformation of these two dual cell chains via estimating the elastic potential energy landscapes of two dual assemblies. For the compression diode, this folding-induced constraint increase the energy barrier for compressing from a certain stable state to another, however, the same constraint does not increase the energy barrier of the opposite extension. Thus, one should apply a large force to compress the chain, but a small force to extend it. As a result, a compression mechanical diode is achieved. This constraint acts the opposite way in extension diode. Then, four prototypes were fabricated to experimentally validate the analytical results. The results of this study can open new avenues towards multi-functional structure and materials systems capable of motion rectifying, wave propagation control, and even mechanical computation.

Keywords: Origami, Multi-stability, Mechanical Diode

Acknowledgements

The author acknowledge the partial support from the National Science Foundation (Award CMMI-1633952, 1751449 CAREER) and Clemson University (via startup funding and the CECAS Dean's Faculty Fellow Award).

Contents

List of Figures

List of Tables

Nomenclature

a_I - Muira-ori sheet I edge

a_{II} - Muira-ori sheet II edge

b_I - Muira-ori sheet I edge

b_{II} - Muira-ori sheet II edge

γ_I - Muira-ori sheet I sector angle

γ_{II} - Muira-ori sheet II sector angle

θ_I - Muira-ori sheet I folding angle

θ_{II} - Muira-ori sheet II folding angle

ϕ_i - Dihedral angles

psi_I - Muira-ori sheet I spine angle

ψ_{II} - Muira-ori sheet II spine angle

L - Individual unit cell length

l_I - Sheet I length

l_{II} - Sheet II length

l_c - Connecting sheet length

L^A - Cell A length

L^B - Cell B length

L^o - outer connecting sheet length

L^t - Dual cell-chain length

$\prod^A$ - Cell A elastic potential

$\prod^B$ - Cell B elastic potential

$\prod^o$ - Outer connecting sheet elastic potential

$\prod^t$ - Dual cell chain total elastic potential

k_i - crease stiffness

k^* - kinematic constraint stiffness

A_1 - Sheet I surface area

A_2 - Sheet II surface area

A_3 - Connecting sheet surface area

F_c^A - Cell A compression reaction force

F_e^A - Cell A extension reaction force

F_c^B - Cell B compression reaction force

F_e^B - Cell B extension reaction force

F_c^C - Dual cell chain with crease-connection compression reaction force

F_c^R - Dual cell chain with rod-connection compression reaction force

F_e^C - Dual cell chain with crease-connection extension reaction force

F_e^R - Dual cell chain with rod-connection extension reaction force

Chapter 1

Introduction and Literature Review

1.1 Introduction

A structure or material system is considered multi-stable if they exhibit more than one stable equilibrium (or stable state) within the deformation range so that each stable sate corresponds to a potential energy minimum [28]. Multi-stability can be used as an alternative mechanism in enabling a wide variety of functionalities such as stiffness adaptation [33], energy harvesting [32] [7]. Origami the ancient art of folding paper into aesthetic shapes has drawn the attention of the researches from various fields like aerospace [45] [27], architecture [43], robotics [29], and biomedical [18] [17] industries.

Recently, origami capability to create programmable and re-programmable systems that can change shape, function and, mechanical properties has opened up innovation doors [10] from macro scale to nanoscale. For example, a sheet, with pre-defined fold lines, capable of reshaping autonomously into different 3D structures was created by Hawkes *etal.* [14], or Marras *etal.* [25] showed that with folding DNA nano-scale mechanisms with programmable mechanical functions can be built.

These structures exhibit unique mechanical properties such as negative Poisson's ratio [22] [39], discrete stiffness jumps [20] [3], elastic multistability [44] [16]. Recent studies have shown that origami-based cellular structures and materials are promising platforms to achieve bi-stability [24]. If the crease bending stiffness between two adjacent sheets in the cellular structure differ notably [27] [43], or its facets are deformed between different configurations [31] [21], the origami structure exhibit multiutility. Moreover, utilizing origami, a three-dimensional shape transformation mechanism, leads to obtaining multi-stability in higher dimensions [41]. This privilege of origami over currently employed bi-stable mechanisms such as the curved beams or their close relatives, prestressed bilayer shells and, axially constrained springs [28] [12], open avenues to create adaptive materials and functional materials [41]. The infinite possibilities of folding combinations [8] [15], and robust manufacturability [35] [30] of folded sheets make them a high potential candidate to construct multi-functional materials. One of the most used multi-stable origami structures is the stacked Miura-ori which is constructed by assembling geometrically compatible Miura-ori sheets along their creases [38]. In stacked Miura-ori, the multi-stability is induced by the Miura-ori sheets considerable stiffness difference [23].

Through the transition to obtaining multi-stability in higher dimensions with origami's 3D nature, the stacked Miura-ori has been shown to exhibit rapid deformation via pressure-induced snapping [43] and elastic modulus programming [26]. In one study, it is observed that the multi-stable stacked Miura-ori exhibits unique asymmetric energy barriers and mechanical diode behavior [41]. Folding induces a kinematic constraint that causes a significant increase in the energy barrier when the structure is being stretched while the required energy for compression does not experience a notable change. Thus, a large amount of force must be applied to extend the stacked Miura-ori, but only a small force to compress it.

In this design, static diode behavior is observable only in the extension direction. This finding has brought up this question that how we can come up with a design to see the diode behavior in compression, and if it is possible to transform it into extension diode with a small change in the designed structure with the existing constituents.

The goal of this research to propose a cellular origami structure capable of exhibiting static diode behavior in compression. The proposed origami unit cell can be counted as a variation of the traditional stacked Miura-ori (Figure 1.1).This dual cell assembly is compared to an electronic diode or a mechanical ratchet. The three structures are designed to rectify the operating direction; The electricity current flow is one-way in the electronic diode, or the rotational movement of the ratchet is unidirectional, and finally the compression diode dual assembly facilitates the deformation in extension direction only.

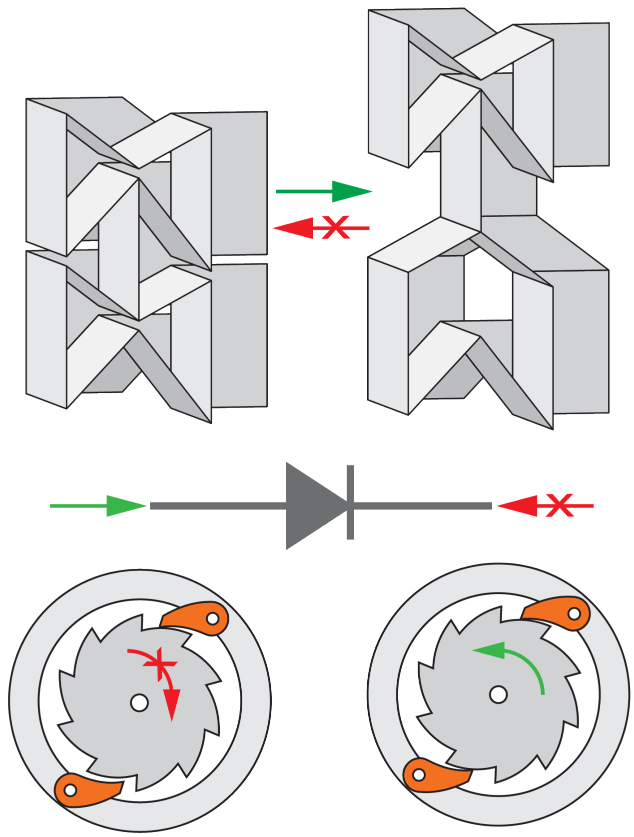

Figure 1.1: The mechanical compression diode design.The dual cell chain is easy to extend but hard to compress. There can be an analogy between this structure and, electronic diode and, mechanical ratchet.

By using the rigid facet and spring hinge assumption the energy landscape of a newly designed origami cellular structure is calculated and it has shown the desired energy asymmetric barrier and static diode behavior. The calculated energy landscape shows that the kinematic constraint induced by folding causes a significant increase in the energy barrier in shifting between two consecutive stable configurations in compression direction, but no notable change in the energy barrier in the opposite switch was noticed. An experimental examination has been conducted to validate the theoretical results.

Followingly, the theoretical model of the extension diode was developed based on the compression diode model (Figure 1.2). The energy landscape of the derivative stacked origami was calculated based on the same assumption of rigid foldability. The energy landscape of the extension diode showed the expected asymmetric energy barrier in the extension direction. Meaning that one should apply a large amount of force to stretch the cellular structure, but a small amount of force to compress it. The attained theoretical results were accompanied by experimental examination, and the extension diode behavior was observed.

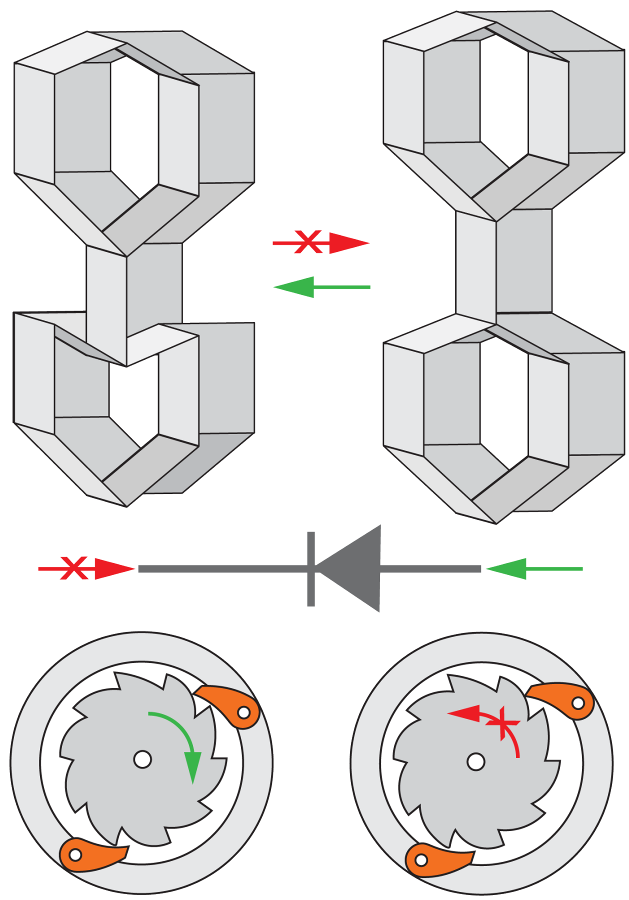

Figure 1.2: The mechanical extension diode design. The dual cell chain is easy to compress but hard to extend. There can be an analogy between this structure and electronic diode and, mechanical ratchet.

One of the potential applications of this static diode is to be deployed in mechanical programming. The current transistor-based computing circuits use multiple inter-connected transistors to create a single Boolean logic gate. These electronic computational components cannot function properly in harsh environments and because of excessive heat dissipation, they demand involved thermal management. Besides, transistor circuits are not capable of dynamically reconfigure their functionality in real-time [5].

The mechanical computing is being investigated by many research groups due to its advantages over its electronic counterparts. For example, in comparison with electronic parts, mechanical parts can resist much higher temperature and radiation exposure [4] [6]. Another advantage of mechanical logic devices they don't need power source because they use energy in mechanical form [36] [40]. Moreover, studies on reversible-computing have suggested that designing a mechanical logic system with small energy dissipation is theoretically possible [19] [11]. Currently, several mechanical computations systems have been introduced. For example, Yuanping Song *etal.* performed Boolean computations based on the mechanical forces and displacements of multi-stable micro-flexures [40]. Raney *etal.* and the coworkers have architected a medium composed of elastomeric bistable beams elements connected by elastomeric linear springs that propagate mechanical signals. This architected structure can be used to design mechanical diode and logic gates [34]. Origami structures have shown a rich potential to be adopted to soft actuation materials and mechanisms [13].

Another potential application of origami mechanical diode is to be integrated into soft robots and materials to serve different tasks. For example, The central unit processing units in soft robots that manage the decision step in the interaction process of the robot with the environment are composed of rigid electronics. Integrating these stiff parts in soft robots is not thoroughly compatible with the compliant body of soft robots. Treml *etal.* and his coworkers have developed a mechanical computation unit with an origami waterbomb as the experimental platform to be Incorporated in soft robots as an solution to the mentioned problem [42]. In what follows, Chapter 2 discusses the mechanics modeling and the theoretical analysis of the compression and tension diodes; Chapter three presents the experimental validation of the theoretical results proposed cellular designs. Chapter four investigates and optimization study on the compression diode unit cell, and eventually in Chapter five concludes this study with summary and future work.

Chapter 2

Mechanics Modeling and Theoretical Analysis of the Mechanical Diode

2.1 Design of The New Cellular Origami Structure

In this study, a new multistable cellular origami structure is introduced. This unit cell is fabricated by stacking geometrically compatible Miura-ori sheets and zigzag shaped "connect sheets" in an alternating arrangement (Figure 2.1.a). By connecting two unit cells via a connecting sheet, the most fundamental multi-stable structure that can exhibit diode behavior is obtained (Figure 2.1.b). The designed unit cell is essentially a variation of a classical stacked Miura-ori [38].

In the unit cell discussed here, the orientation of the Miura-ori with respect to each

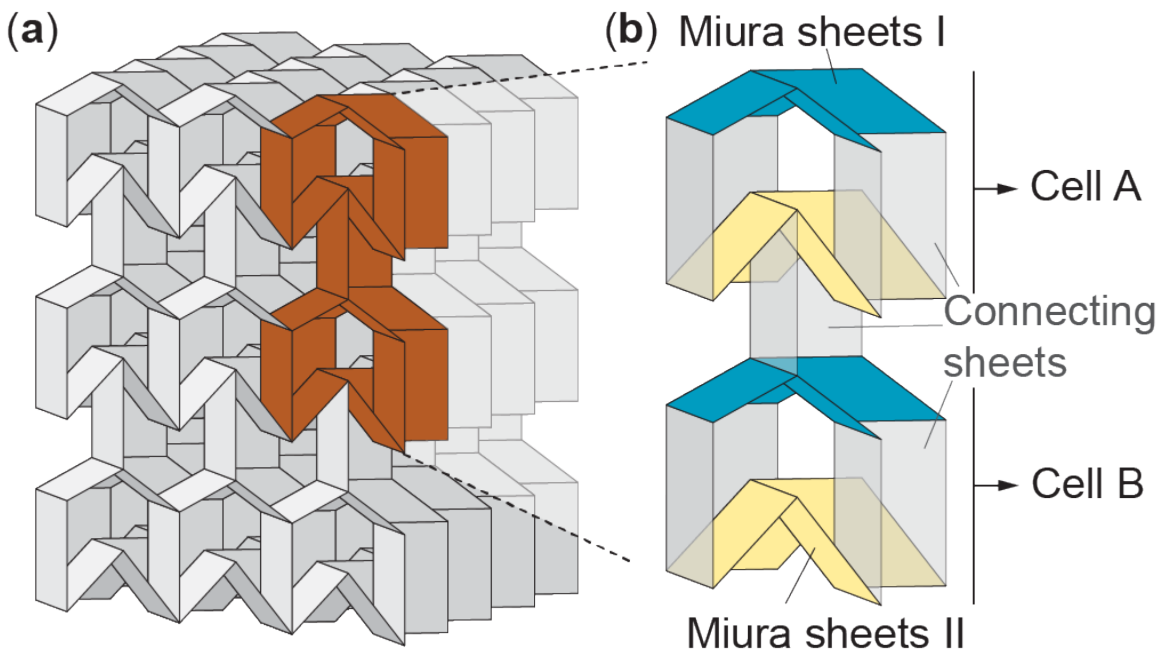

Figure 2.1: Design of the new multistable stacked origami cellular structure. (a) An overview showing the alternating sequence of different Miura-ori sheets and zig-zag “connect sheets”.

other is flipped. More clearly stated, the Miura-ori sheet with the bigger dimension in one edge, also referring to as sheet II, is reversed in the new design (Figure 2.2).

The new unit cell still follows the rigid-folding kinematics of traditional Miura-ori [38]. The crease design of a unit cell is determined by crease lengths (a_I,b_I, a_{II}, b_{II}, l_c) and the sector angles (γ_I, γ_{II}) (Figure 2.3.a). Here, subscript I and II denote the two different Miura-ori sheets in a unit cell and l_c is the length of the connecting sheet. To satisfy the geometric compatibility the following restraints [38] should be imposed on these parameters values :

$$b_{\mathrm{II}} = b_{\mathrm{I}}, \tag{2.1}$$

$$\frac{\cos \gamma_{\mathrm{II}}}{\cos \gamma_{\mathrm{I}}} = \frac{a_{\mathrm{I}}}{a_{\mathrm{II}}}. \tag{2.2}$$

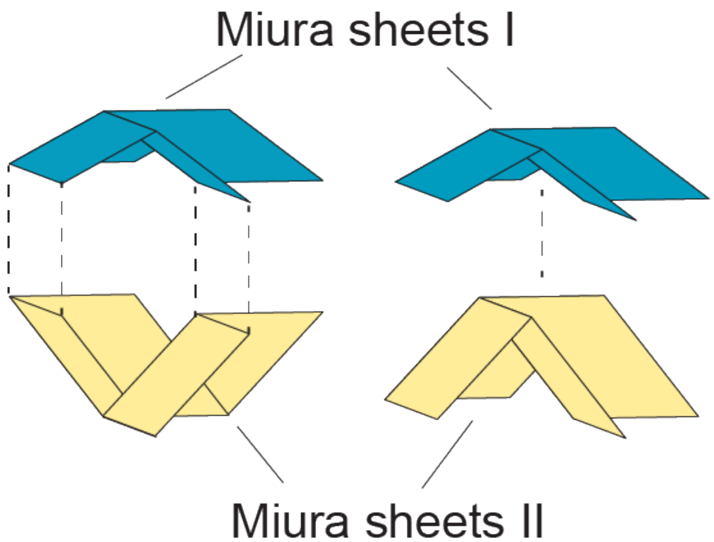

Figure 2.2: (a) Miura-ori sheet II is flipped in the new compression diode unit cell. (b) The arrangement of sheet I and II with respect to each other in traditional stacked Miuor-ori

To describe the external geometry of a unit cell during rigid-folding, one can use dihedral folding angles θ_I and θ_{II} defined between the facets of the two Miura-ori sheets and the x-y reference plane, respectively (Figure 2.3.b).

In the geometric design, it assumed that the unit cell ideally satisfies the rigid-folding condition, which is essentially a one-degree-of-freedom motion [9]. This condition is stated by the following relationship between the two sector angles and the folding dihedral angles [38]:

$$\cos\theta_{\mathrm{I}}\tan\gamma_{\mathrm{I}} = \cos\theta_{\mathrm{II}}\tan\gamma_{\mathrm{II}}. \tag{2.3}$$

The summation of the different components of the unit cell gives the total length of the unit cell.

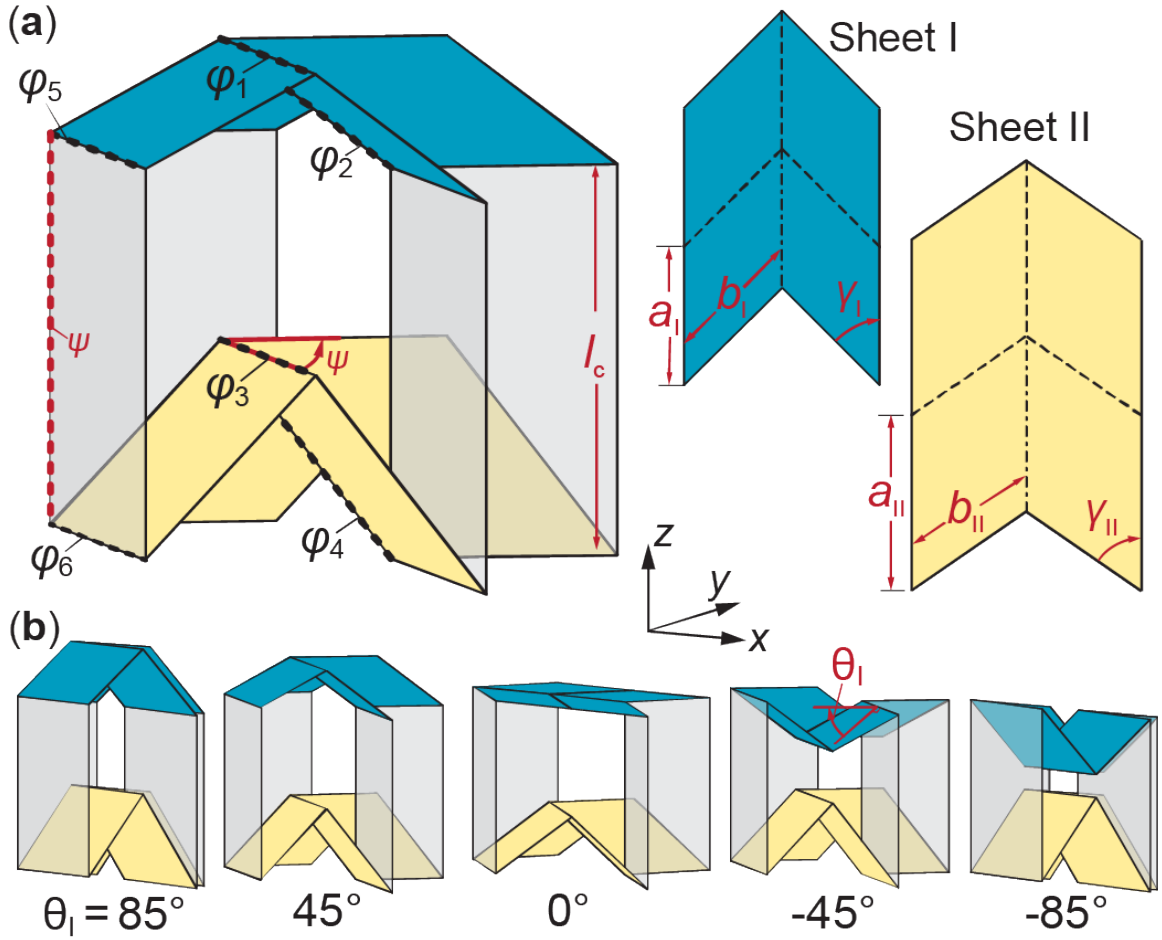

Figure 2.3: Detailed design of a unit cell in this study. (a) Φ_i (I $= 1 \ldots 6$) are unique dihedral angles between two adjacent facets along the difference creases. ψ_i is the spine angle, which is also the dihedral angle of in the connect sheet. The two drawings on the right show the design of Miura-ori sheets

$$L = l_{\mathrm{I}} + l_{\mathrm{II}} + l_c, \tag{2.4}$$

Where l_I and l_{II} are the length of the two constituent Miura-ori sheets respectively.

To describe dihedral folding angles between the facets in the connect sheet, a spine angle can be defined [9]:

$$\psi = 2\tan^{-1}(\cos\theta_{\mathrm{I}}\tan\gamma_{\mathrm{I}}), \tag{2.5}$$

At it was mentioned, it is assumed that the unit cell facets are ideal rigid the crease lines act as perfect hinges with prescribed torsional stiffness. This assumption satisfies the rigid-folding condition kinematics. Thus, the total elastic potential energy of the structure can be calculated using the following equation [1]:

$$\Pi = \frac{1}{2}k_i(\varphi_i - \varphi_i^o)^2 + \frac{1}{2}k_c(\psi - \psi^o)^2, \tag{2.6}$$

Where $_i$ is the dihedral crease opening angle denoted in Figure 2.3.a; These angles measure the angles between intersecting planes forming the compression diode unit cell's geometry, and φ_i^o is the initial value of the corresponding dihedral angle (it is worth to remind that all the angles defining the unit cell's geometry are functons of the folding angle θ_i.). k_i is the corresponding torsional spring stiffness in the connect sheets. The initial stress-free configuration angles are denoted by subscripts o. The crease opening angles are the function of independent variable θ_I and can be described using the following equations: (equations 2.8, 2.9 and 2.10 are adapted from previous publications [23]):

$$\varphi_1 = \pi - 2\theta_{\mathrm{I}}, \tag{2.7}$$

$$\varphi_2 = 2\sin^{-1}\left(\frac{\cos\theta_{\mathrm{I}}}{\sqrt{1-\sin^2\theta_{\mathrm{I}}\sin^2\gamma_{\mathrm{I}}}}\right), \tag{2.8}$$

$$\varphi_3 = \pi - 2\cos^{-1}\left(\tan\gamma_{\mathrm{II}}\tan^{-1}\gamma_{\mathrm{I}}\cos\theta_{\mathrm{I}}\right), \tag{2.9}$$

$$\varphi_4 = 2\sin^{-1}\left(\frac{\sin\gamma_{\mathrm{I}}}{\sin\gamma_{\mathrm{II}}}\sin\frac{\varphi_2}{2}\right), \tag{2.10}$$

$$\varphi_5 = \frac{\pi}{2} + \theta_{\mathrm{I}}. \tag{2.11}$$

$$\varphi_6 = \frac{\pi}{2} - \theta_{\mathrm{II}}. \tag{2.12}$$

Although the torsional springs added to the creases are linearly elastic as can be seen in equation 2.6, the correlations between folding and external deformation are geometric and strongly nonlinear. The desired diode behavior originates from this nonlinearity. k_i and k_I are the crease torsional stiffness per unit length of the Miura-ori sheet I and II, respectively, and k_c is the crease torsional spring stiffness per unit length of the connecting sheet. The stiffness coefficients in equation 2.6 are $k_1 = 2k_{\mathrm{I}}b_{\mathrm{I}}, k_2 = 2k_{\mathrm{I}}a_{\mathrm{I}}, k_3 = 2k_{\mathrm{II}}b_{\mathrm{I}}, k_4 = 2k_{\mathrm{II}}a_{\mathrm{II}}, k_5 = 4k_c b_{\mathrm{I}}, k_6 = 4k_c b_{\mathrm{I}}$, and $k_c = 2k_c l_c$, where the numerical coefficients in these equations show determines the similar creases in one unit cell.

In order to achieve bi-stability in a stacked Miura-ori unit cell , the stiffness of the larger sheet II should be much higher than the crease stiffness of the sheet I and the connecting sheet (also known as $k_{II} > k_I$ and k_c) . Moreover, the initial stress-free folding configuration should drift from 0 [23]. As it is shown in Figure 2.3-b different values of θ_I can be chosen as the initial value of this angles to enable bi-stability except for $\theta_I = 0$. Figure 2.4 illustrates the energy landscape of two unit cells (referred to as cell A and B hereafter) of the geometric parameters value of $a_{\mathrm{I}} = b_{\mathrm{I}} = 2\mathrm{cm}$,$a_{\mathrm{II}} = 1.25a_{\mathrm{I}}, \gamma_{\mathrm{I}} = 45°, l_c = 2.5\mathrm{a}_{\mathrm{I}}, k_{\mathrm{I}} = k_c$, and $k_{\mathrm{II}} = 20k_{\mathrm{I}}$ (equation 2.6). The initial dihedral angle of cell A is chosen to be 60 and cell B to be -60 degrees.

The two potential energy wells of each cell (Figure 2.4) exhibit the bi-stability of this group of geometric design parameters. In purpose of more clarity, the positive folding angle of sheet I is denoted as state (1) and the negative stable configuration as (0) so that the unit cell has the shortest length L at state (0). Throughout the entire

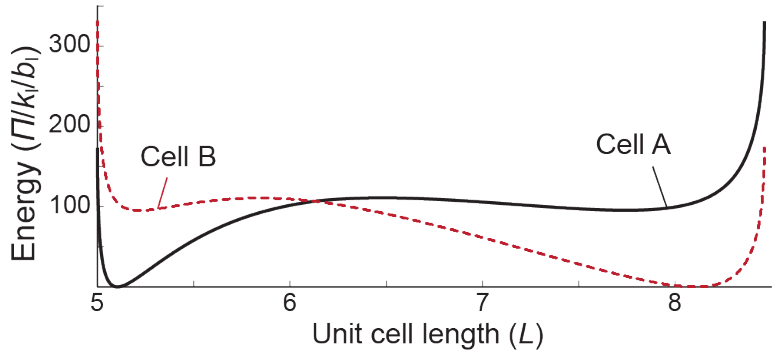

Figure 2.4: The energy landscape of the two unit cells used in this study.

thesis, these design values are kept the same consistently, unless noted otherwise. The initial dihedral angle of cell A is chosen to be 60 and cell B to be -60 degrees. These stress-free configurations dictate the force relation between the individual cells as follows: $F_c^A < F_c^B$, and $F_e^B < F_e^A$.

After formulating the unit cell external geometry and potential energy, the overall energy and dimension of the dual cell assembly can be calculated as:

$$\Pi^{\mathrm{t}} = \Pi^{\mathrm{A}} + \Pi^{\mathrm{B}} + \Pi^{0}, \tag{2.13}$$

$$L^{\mathrm{t}} = L^{\mathrm{A}} + L^{\mathrm{B}} + L^{0}. \tag{2.14}$$

Π^A, and Π^B are the strain energy of the unit cell A and B with the definition stated in equation 2.6. Π^0 is the strain energy of the connecting sheet between the two unit cells and defined as:

$$\Pi^{0} = \frac{1}{2}k^{*}\left(\psi^{\mathrm{A}} - \psi^{B}\right)^{2}, \tag{2.15}$$

Where k^* is the constraint stiffness of the “connecting sheet”. This parameter is the key element of this study since it quantifies the strength of kinematical constraint induced by folding. Ideally, if the rigid-folding assumption is observed (aka. all facets in the dual cell chain are fully rigid and all creases act perfectly as hinges), the spine angles of the two unit cells should be equal. ($\psi_A = \psi_B$). In this way, the admissible deformations of the dual-cell chain are restricted to the "kinematic paths" shown in Figure 2.5.a.

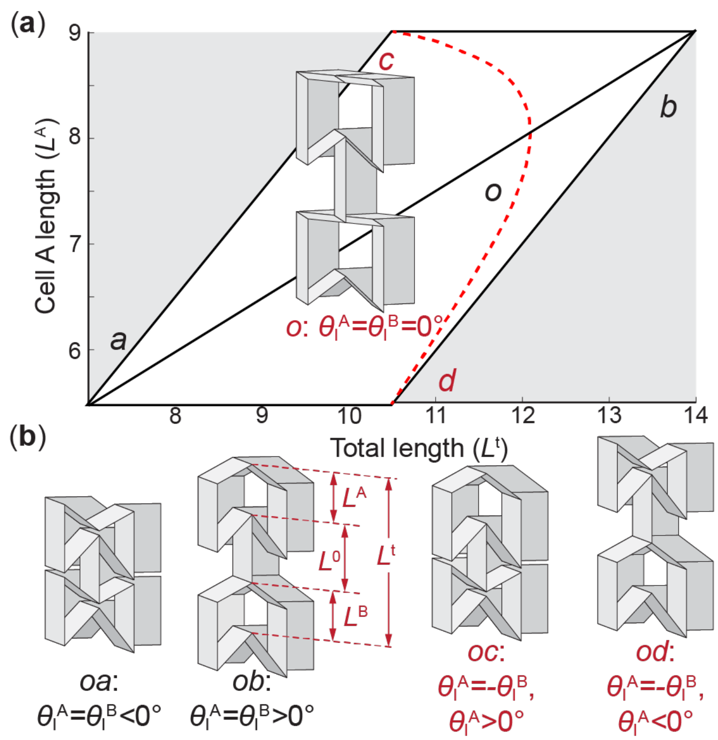

Figure 2.5: Kinematic properties of the compression diode structure due to the folding induced constraint (or the lack of). (a) Admissible deformation of the dual cell assembly. The two kinematic paths based on ideal rigid-folding condition are shown by the solid and dashed curves. The gray area represents deformations that are not kinematically admissible. (b) The geometry of the dual cell assembly at different locations along these to kinematic paths.

In ideally rigid-folding condition, one possible path would be $\theta_I^A = \theta_I^B$, and the other path be $\theta_I^A = -\theta_I^B$. However, the facets are not ideally rigid, and the creases do not behave like perfect hinges. More specifically, the facets have small bending and creasing wrapping will take place. Thus, there would be some mismatch between the two spine angles of the two unit cells. In conclusion, the configuration of the dual-cell assembly can occur at any point within the parallelogram shown in Figure 2.5.a. This deviation from ideal rigidity can apply additional elastic potential energy that can be characterized by the constraint stiffness k^*.

In the next sections, first, the nonlinear elastic behavior of dual-cell assembly in the absence of the kinematic constraint stiffness ($k^* = 0$) is examined, and then the situation at which the kinematic strain energy is added to the system is studied.

2.2 Diode effect in compression

Figure 2.6.a illustrates the total energy landscape of the dual cell chain according to equation 2.13 with $k^* = 0$. This scenario represents a hypothetical case in which the sheet that connects the two cells are soft so that it does not provide any resistance to the mismatch between the spine angles of the two cells (ψ^A and ψ^B) . The "equilibrium paths" corresponding to the potential energy minima at a given total length can be determined, and the dotted line shows the potential energy maxima at that length. During deformation (changing from the minimum length to maximum length) the dual cell assembly would pave these minima paths. Here, the continuous equilibrium path that connects the three stable states of "0-0", "0-1", and "1-1" is of interest. The energy landscape of the dual-cell assembly along this path is plotted in Figure2.6.b.

The extension energy barrier (ΔE) for shifting from "0-0" stable state to "0-1" stable state and the compression energy barrier for the opposite switch ΔC can be seen in

Figure2.6. The corresponding reaction force can be calculated as the variation of total potential energy with respect to the change in total length:

$$F = \frac{\partial \Pi^{\mathrm{t}}}{\partial L^{\mathrm{t}}}. \tag{2.16}$$

The reaction force corresponding to the continuous equilibrium path is shown in Figure 2.6.c. Based on this plot, two important forces can be calculated. One is the critical reaction force (F_e) during switching from "0-0" stable configuration to "0-1" stable configuration. The other important force (F_c) is the critical reaction force to make the opposite switch (from "0-1" to "0-0") happen. Essentially, (F_e) is the force required to stretch the dual-cell chain from "0-0" to "0-1", and (F_c) is the needed amount of force to compress the structure back to "0-0" state.

The discussed scenario above showed a hypothetical case in which the connecting sheet between the two cells are soft enough that it does not impose any kinematical resistance. However, to exhibit the realistic structural behavior of the assembly under imposed kinematic constraint, it should be assumed that the connecting sheet in between is not soft (stiffer connection results in more resistance against the mismatch), and displays resistance to the mismatch between the spine angles during deformation (ψ^A, and ψ^B). In terms of theoretically modeling this case, the magnitude of parameter k^* is crucial here. Figure 2.7 illustrates the potential energy landscape and reaction force of the dual-cell assembly along the continuous equilibrium path when the constraint stiffness k^* increases (the dotted lines in the first row of Figure 2.7 correspond to the potential energy maxima at a given length). As the constraint increases, the potential energy barrier for compression switch from "0-1" stable state to "0-0" increases significantly, but the energy barrier for the extension switch does not increase by the same degree. Moreover, when the kinematical stiffness reaches a threshold value ($\frac{k^*}{k_I} = 140$ in this case study), the initially continuous equilibrium path that connects three stable states splits into two separate ones (see the first two rows of Figure 2.7.b and .c). As a result, when the dual structure is extended from the "0-0" stable state, it will deform to point P at the end of one equilibrium path and then "leap" to the other path. In the compressing direction from "0-1" to "0-0", the dual structure deforms to Q first before leaping (see the insert figure in the first row in Figure2.7.c). The asymmetry in the energy barrier caused by kinematic constraint resulted from folding makes the required energy to reach mentioned leaps significantly different between the extension and compression direction.

By examining the changes in critical forces as the kinematical constraint k^* increases, the presence of the asymmetric energy barrier can be further emphasized (the third row of Figure 2.7). From Figure 2.7, one can see that with the increase of k^*, the required force to compress the dual structure from "0-1" stable state to "0-0" stable state is notably increasing while the required force to extend it back to "0-1" does not change much (Table 2.1).(Section 2.2 and Section 2.3 are published [1].)

Table 2.1: The normalized critical forces in the extension and compression switches between the (00) and (01) stable states based on the reaction force plots in Figure 6 and 7.

$\frac{k^*}{k_I}$	$\frac{F_e}{k_I}$	$\frac{F_c}{k_I}$
0	26.5	-91.7
50	32.5	-467.3
140	36.3	-1261.7
600	39.9	-2079.7

2.3 Diode effect in extension direction

In the unit cell of the extension diode, the orientation of sheet II is flipped. In other words, the orientation of sheet I and sheet II with respect to each other is the same as the traditional stacked Miura-ori. The dual cell chain of extension diode can be seen in Figure 2.8. The same as the compression diode unit cell, this unit cell also is consisted of geometrically compatible Miura-ori sheets and satisfies the rigid folding condition (equations 2.1 and 2.2). This change did not change the relations between the individual cells reactions forces ($F_c^A < F_c^B$, and $F_e^A > F_e^B$). Moreover, the three achievable stable states by global extension or compression are the same as the compression diode.

In ideal rigid condition, where k^* is infinitely high, there is no mismatch between the spine angles. In this way, the admissible deformations of the extension dual cell chain are bounded to the "kinematic paths" shown in Figure 2.8.a . The total length of the dual stricture can be defined as follows (Figure 2.8.b):

$$L^{\mathrm{t}} = L^{\mathrm{A}} + L^{\mathrm{B}} + L^{0}. \tag{2.17}$$

One should note that the unit cell total length (cell A or B) is the summation of the sheet I and sheet II and the connecting sheet length while the unit cell length in the compression diode is calculated using equation 2.18:

$$L^{A} = L^{B} = L^{I} + L^{II} + L^{c}. \tag{2.18}$$

The total potential energy of the dual cell assembly is calculated with the same approach used for the compression diode. The changes in the energy landscape of this structure with the increase in k^* can be seen in the first row of Figure 2.10. The energy of the equilibrium path and the corresponding reaction force are shown in the second row and third row of Figure 2.10 respectively.

As k^* increases, the required force to switch from "0-1" to "1-1" stable configuration is increasing while, the reaction force for shifting from "1-1" back to "0-1" is not changed as much. Moreover the extension reaction force of changing from "0-0" to "1-1" does not experience a large change. Similarly with extension compression diode, when the reaches k^* the threshold ($\frac{k^*}{k_I} = 220$), the continuous equilibrium path splits into two separate path (Figure 2.10.b). When the dual structure is extended from the "0-1" stable state to "1-1, it will deform to point Q at the end of one equilibrium path and then "leap" to the other path. In the compressing direction from "1-1" to "0-1", the dual structure deforms to P first before leaping (see the insert figure in the first row in Figure 2.10.c). With a closer look at the second row of Figure 2.10, it is evident that the extension energy barrier between state '0-1' and '1-1' is growing as k^* increases.However, this growing rate is not observed in the compression energy barrier between '1-1' and '0-1' stable configurations. Thus, to switch from '0-1' to '1-1' stable state, a larger force is required with the increase of k^*. The second row of Figure 2.10 also shows that the required force for compressing the structure from '1-1' to '0-1' is not increased much. In conclusion, this dual cell structure exhibits diode behavior in extension direction, a structure hard to extend but, easy to compress.

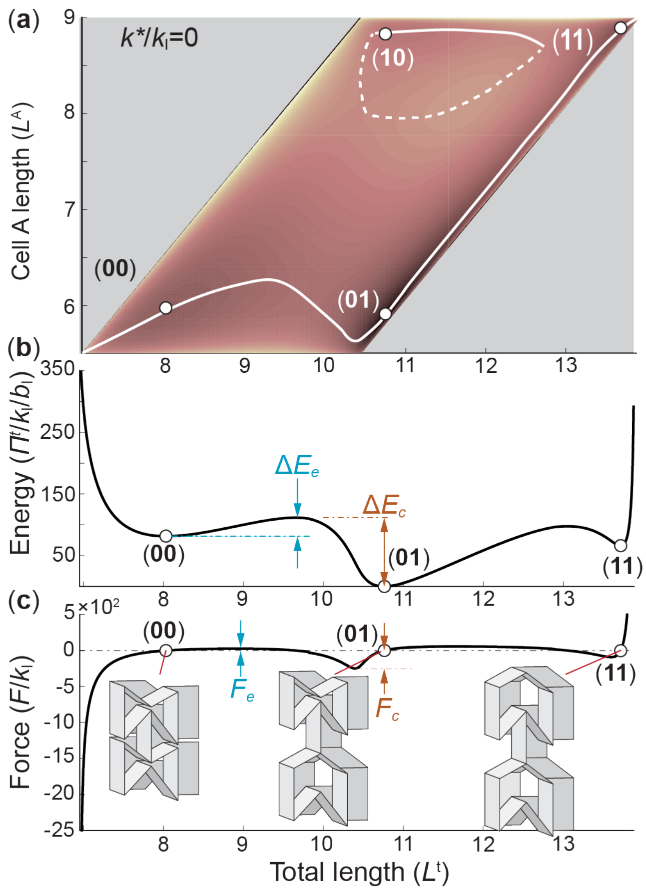

Figure 2.6: Mechanics of the dual-cell assembly assuming zero constraint stiffness k*: (a) the total potential energy landscape, (b) the equilibrium path, and (c) the reaction force along the equilibrium path. The colormap in (a) represents the total potential energy, darker color means lower energy. It is worth nothing that in this figure and the following Figure 6, only the equilibrium path containing the (00), (01), and (11) stable states are shown in the energy landscape and reaction force plots. This is because the (10) state is not achievable by global extension or compression.

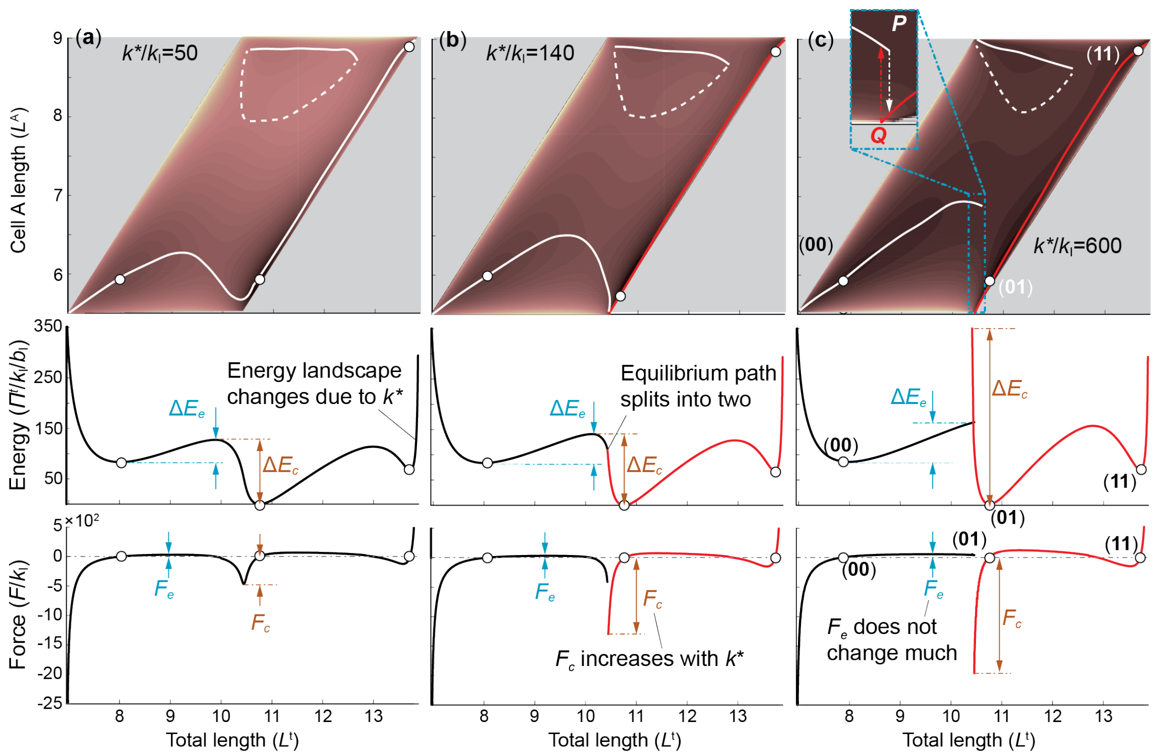

Figure 2.7: The energy contours (first row), energy landscapes (second row), and the reaction force (third row) corresponding to an increasingly stronger folding induced kinematic constraint: (a) $\frac{k^*}{k_I} = 50$, (b) $\frac{k^*}{k_I} = 140$, and (c) $\frac{k^*}{k_I} = 600$. The "leap" between the equilibrium paths are illustrated as dashed arrows in the insert figure in the first row of (c).

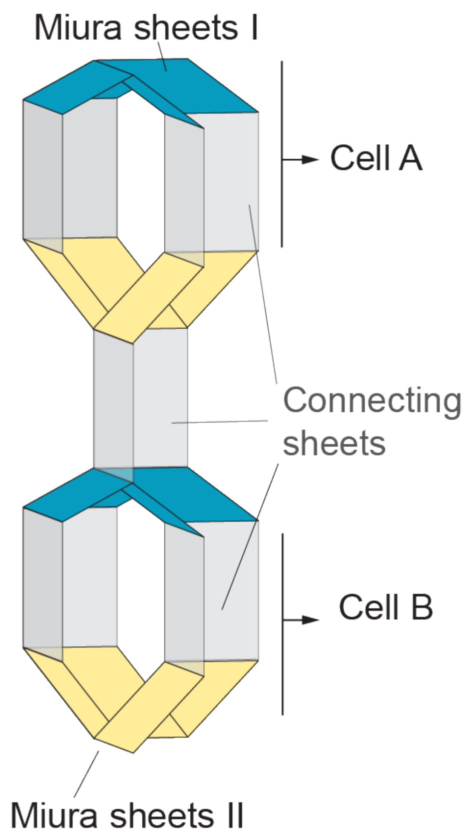

Figure 2.8: The dual cell chain of the extension mechanical diode. Miura-ori sheet II is flipped back to the configuration it poses in traditional stacked Miura-ori.

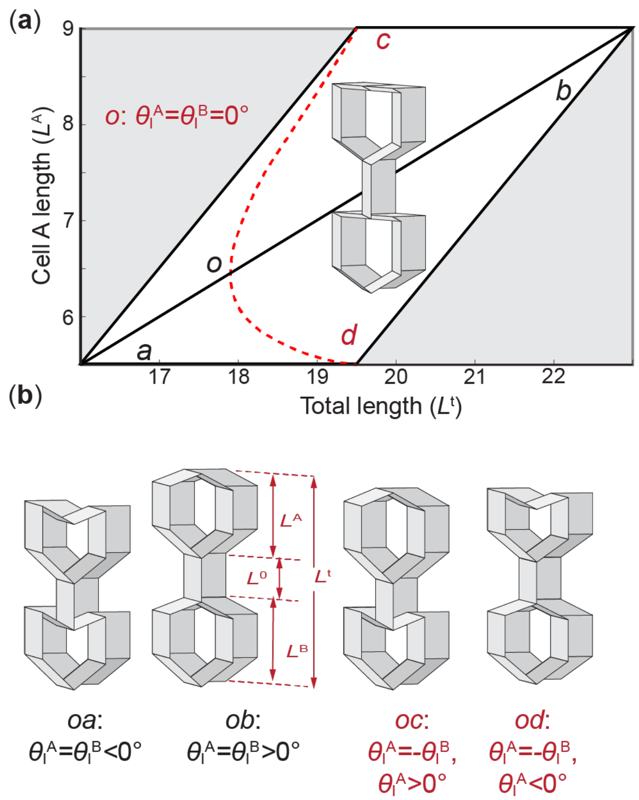

Figure 2.9: Kinematic properties of the extension diode structure due to the folding induced constraint (or the lack of). (a) Admissible deformation of the dual cell assembly. The two kinematic paths based on ideal rigid-folding condition are shown by the solid and dashed curves. The gray area represents deformations that are not kinematically admissible. (b) The geometry of the dual cell assembly at different locations along these to kinematic paths.

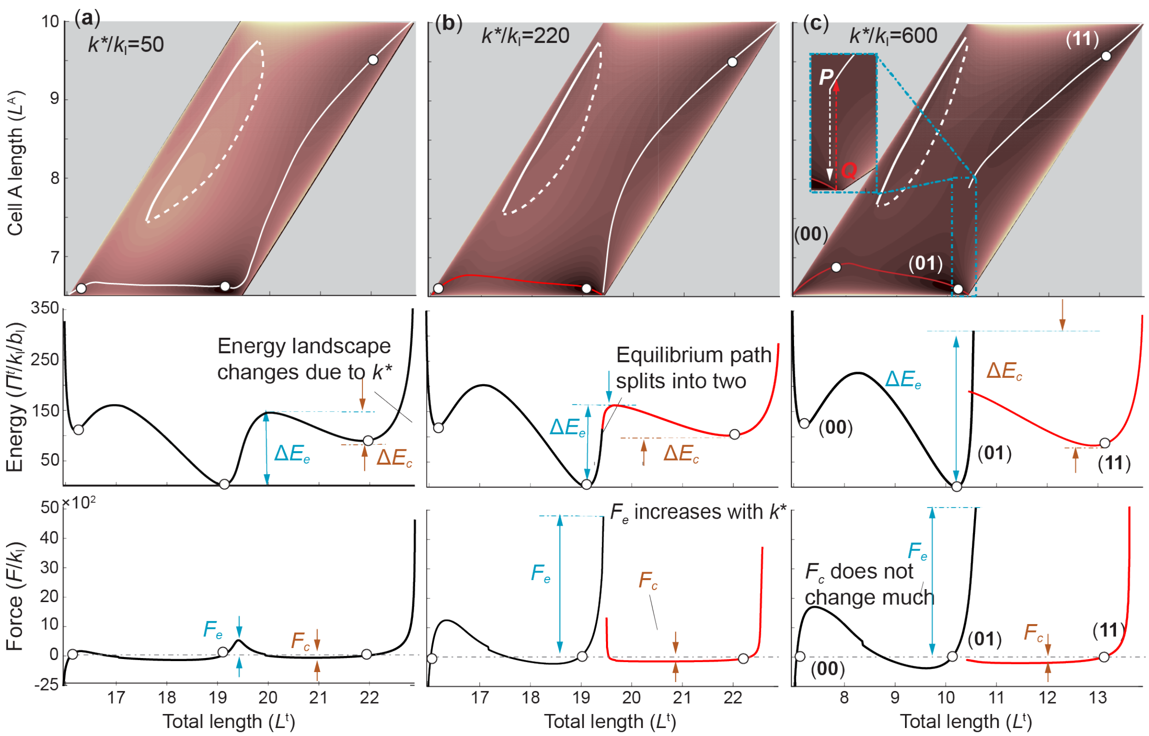

Figure 2.10: The energy contours (first row), energy landscapes (second row), and the reaction force (third row) corresponding to an increasingly stronger folding induced kinematic constraint: (a) $\frac{k^*}{k_I} = 50$, (b) $\frac{k^*}{k_I} = 220$, and (c) $\frac{k^*}{k_I} = 600$. The "leap" between the equilibrium paths are illustrated as dashed arrows in the insert figure in the first row of (c).

Chapter 3

Experimental Investigation of the Compression and Extension diode

3.1 Experimental observation of the diode behavior in compression

After numerous modifications, a carefully designed prototype was fabricated to experimentally validate the analytical results. The patterns of the smallest components of the geometry including the parallelograms of sheet I and II, and the connecting sheets were designed in SolidWorks^{TM}. (The drawings can be found in the appendix) In the rigid folding condition, the planes are ideal rigid. In order to make the experimental setup as close to the rigid folding assumption as possible, fatigue-resistant 301 stainless steel spring temper sheet of 0.01" thickness was used to cut the parts from. This steel provided enough rigidity to the experimental setup to satisfy the rigid folding condition up to a reasonable extent. The parts were water-jet cut, and two similar unit cells were fabricated using adhesive UHMW Polyethylene film of .005" thick. One of the main issues in developing the experimental setup was to find the proper method of fabricating the dual assembly to achieve an ideal multi-stable force-displacement curve. For example, initially the UHMW film was attached on both sides of the cut parts to assemble the dual chain setup. In order to archive a multi-stable measured F-D curve, one should minimize the amount usage of the UHMW adhesive film, specially on the crease regions. In another unsuccessful attempt, the dual assembly parts were broken down to smaller subsets to be fabricated separately and attached together to build the final structure. This method required using extra adhesive film resulting in failure in obtaining proper curves. Eventually, a fabrication process was designed that gave better multi-stable force-displacement curves (Appendix A). The weakness of this process shows itself in experimental investigation of the diode behavior ($k* > 0$). This method can not deliver strong enough connection between the two unit cells when they are connected to each other along their zig-zag creases to represent the added kinematical stiffness $k*$.

For mounting the unit cells to the Universal Tensile Tester, an additional part was designed, and water-jet cut on the from the same materials and was attached to the assembly on carefully determined places on the unit cells. Beside this steel part, a customized connector was 3D printed. After many modifications, the best design for the 3D printed connectors was used to enable the structure to be mounted on the machine.

As it was mentioned above, for a stacked Miura-ori unit cell to be bi-stable, the torsional stiffness of certain creases of the unit cell should be notably higher than the other creases. The two adjacent creases on one side of the connecting sheets were chosen to add the stiffness. Many different metals with different thicknesses were used to choose the one that delivers the best experimental results. For example, the thickness of 0.007 18-8 stainless steel was not strong enough and deformed instantly after one loading cycle, and could not maintain the elastic behavior; Or the thickness of 0.009 of the same steel was too strong for the force scale of the designated experiment and the delicacy of the fabricated setup. Finally, the 18-8 stainless steel shim Stock (0.008" thickness) was employed to add the torsional stiffness on the creases of connecting sheets. This thickness provided enough strength, and at the same time maintains its elastic spring behavior during deformation. The rectangle parts from shim stock in $2.5cm \times 3cm$, were bent into equal angles to be attached on the creases. to avoid any loss of accuracy in the experiment, the angles of all the springs must be as equal as possible. In order to obtain the best consistency, a pair of fixtures with the mating surfaces angle of $65°$ was cut.

Two sets of experiments were conducted. In the first experimental setup, the two unit cells were simply connected to each other in series using M6 rigid rod with a balanced internal force (Figure 3.1.a). For the second test set, the two cells were connected to each other along their zig-zag crease lines by adhesive films. This setup is consistent with the stacked origami construction shown in Figure 3.1.b. In both sets, the arrangement of the cell is in a way that cell B is always on top.

Several single tension and compression load cycles, using the displacement control method, were conducted with the two setups. The increase in the compression force in crease connection in comparison with rod connection was noticed in all of them consistently. In what follows, a pair of numbers (i-j) is used to represent the stable configuration of Cell A and B respectively. All the tests were done in a way that the dual-cell chain is first compressed from the "convex- convex" (i.e. 1-1) stable config-

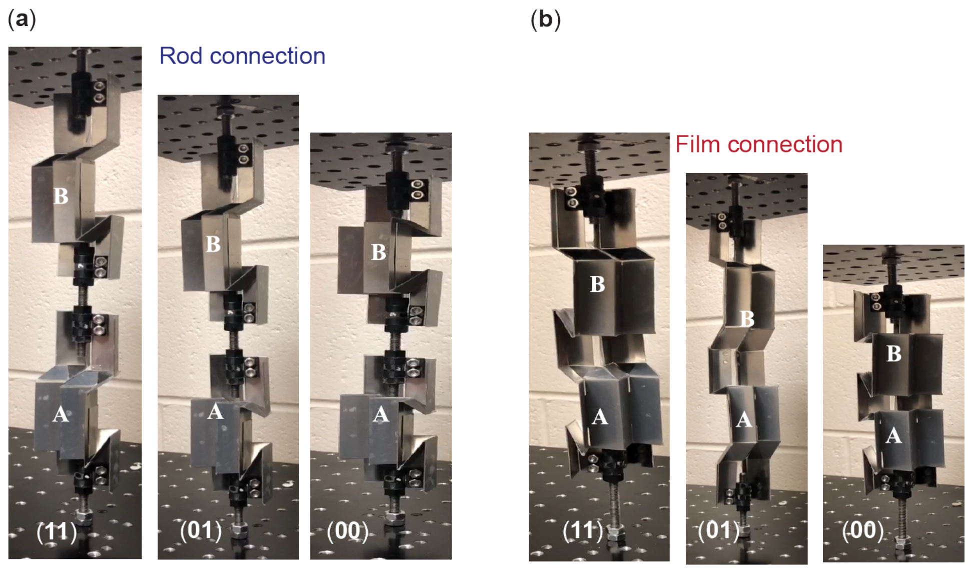

Figure 3.1: The photos of the rod-connected test (a) and crease-connected test of compression diode dual cell-chain (b) show the three stable states ('1-1','1-0', and '0-0')

uration to the "concave-concave" (i.e. 0-0) state and extended back to 1-1 state. The force-displacement graph of one test is shown in Figure 3.2. The noticeable hysteresis in the experimental graphs is due to using adhesive films. After the completion of half of the loading cycle (compression direction), this film goes through plastic deformation and does not provide the desired elastic behavior.

The crosshead speed of this test was 0.08 mm/s. Four different stable configuration combinations are possible for the dual-cell chain: '0-0', '0-1', '1-1', and '1-0'. These switches are evidenced by the negative slopes in both theoretical and experimental force-displacement curves (i.e. negative stiffness). The theoretical model depicts that the relation between the individual cells critical forces is as follows: $F_e^A > F_e^B$ and $F_c^A < F_c^B$. This relation needed to beheld in the experimental setup as well. Experimentally, this relation could be applied by attaching proper numbers of steel stripe on both cells with a certain proportion. It was chosen to attach 4 stripes on

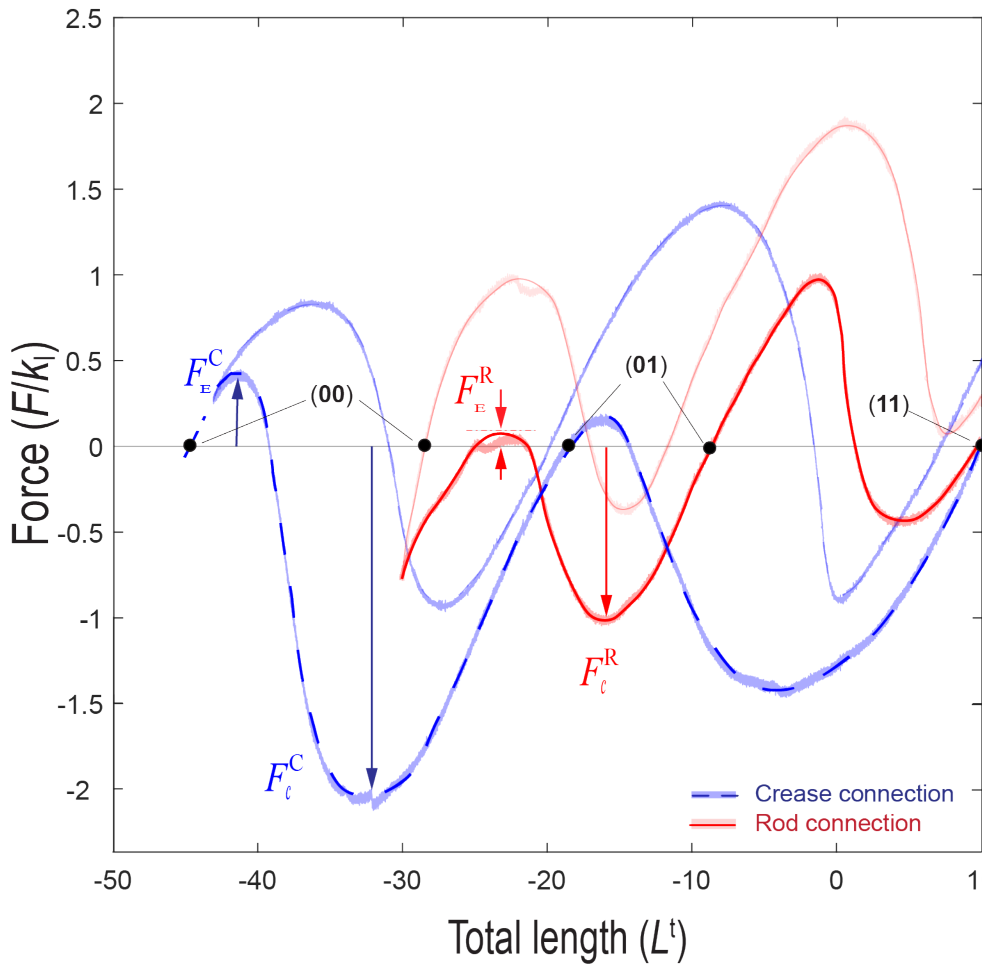

Figure 3.2: Compression and tension tests on compression diode dual-cell chain prototypes with rod connection (red curve) and crease connection (blue curve).

Cell B and 2 stripes on Cell A to achieve the desired force relationships.

The snapping sequence of the dual-cell chain is dictated by this relation both in compression and tension. Thus, only the first three of the possible combinations are achievable via displacement control. In other words, since the critical compression force of Cell B is higher than that of Cell A. '1-0' combination is not attainable. In conclusion, during compression, always Cell A nests in first because of its critical force for snap-through (F_c^A) is lower than that of the top Cell B (F_c^B), and during tension, Cell A bulges out first and then Cell B. Regardless of the inter-cellular connection, the switching sequence in both compression and tension is dictated by the individual cells force relation. In compression, the switching sequence is '1-1','0-1','0-0', and in the tension is '0-0', '0-1', '1-1'. The experimental force-displacement curves of Cell A and B are shown in Figure 3.3.

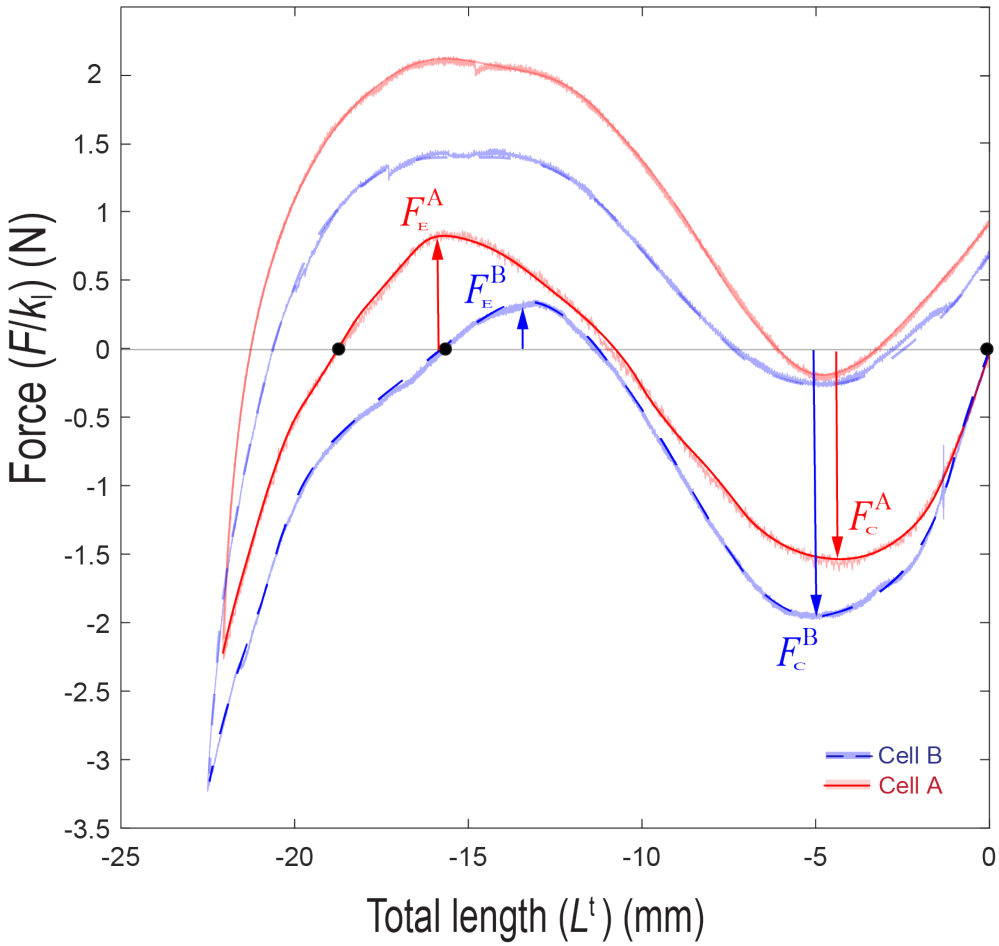

Figure 3.3: Measured force-displacement curves of the two unit cell prototype of the compression diode.

With a comparison of the measured force-displacement curves of the two sets in Figure 3.2, it can be seen that the compression force from switching (01) to (00) is increased in the second setup (crease connection) while no notable increase was seen in extending from '0-0' to '0-1'. This experimentally validates the diode behavior that was noticed in analytical results. However, not much increase was noticed from switching from '1-1' to '0-1'. (The critical forces of the dual chain are denoted with 'F' and 'R' superscript that are referring to crease (film) connection and rod connection, respectively). More specifically, in film connection, the required force to switch from "0-1" to "0-0" was 1.9 N and in rod connection was 1 N.

3.2 Experimental observation of the diode behavior in extension

In the previous sections, the extension diode behavior obtained from the analytical model. It was necessary to experimentally observe diode behavior in extension. The same assembly was used for this experiment with a slight variation in the Sheet II configuration. To obtain the proper setup, the Sheet II of each cell was flipped. That is the only change applied to the compression diode assembly (Figure 3.4).

According to the theoretical model, the same relation between the individual cells critical forces is held and that is,$F_e^A > F_e^B$ and $F_c^A < F_c^B$. The Force-Displacement curve of the individual cells is shown in Figure 3.5. It is evident from the graph that the experimental setup is properly set to satisfy the desired force relation.

Similarly, with compression dual structure, the extension dual-chain poses four possible stable states regardless of the inter-cellular connection: '0-0', '0-1', '1-1', and '1-0'. Again, due to the assigned force relation, only the three stable arrangements are achievable via the displacement-control method (Figure 3.6).

The extension loading starts with the assembly at the 'convex-convex' configuration.

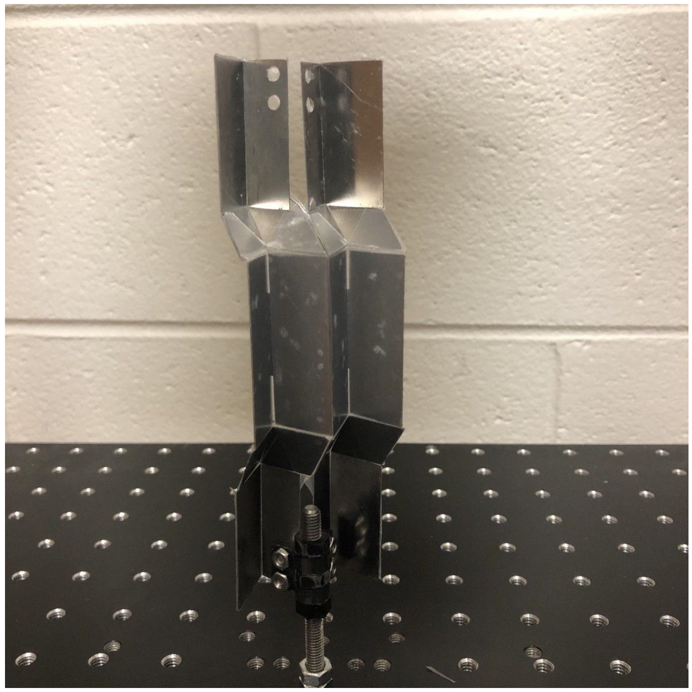

Figure 3.4: The extension diode individual cell prototype

That relation incurs a switching sequence of '0-0' to '0-1' to '1-1' during extension, and by the end of compression loading, the structure goes back to 'convex-convex' configuration. More specifically, Cell B bulges out first and then Cell A during extension, and Cell A nests in first and Cell B followingly (Figure 3.7).

Figure 3.6 shows that in crease-connected setup (blue curve), the required force to extend the dual cell assembly from '0-1' to '1-1' is higher than the needed force to apply this switch in the rod-connected . More specifically, in film connection, the required force of going from '0-1' to '0-0' is 2.1 N, and in the rod connection 1.5 N However, not much difference in magnitude of tension critical force of switch between '0-0' and '0-1' is seen (Figure 3.6).

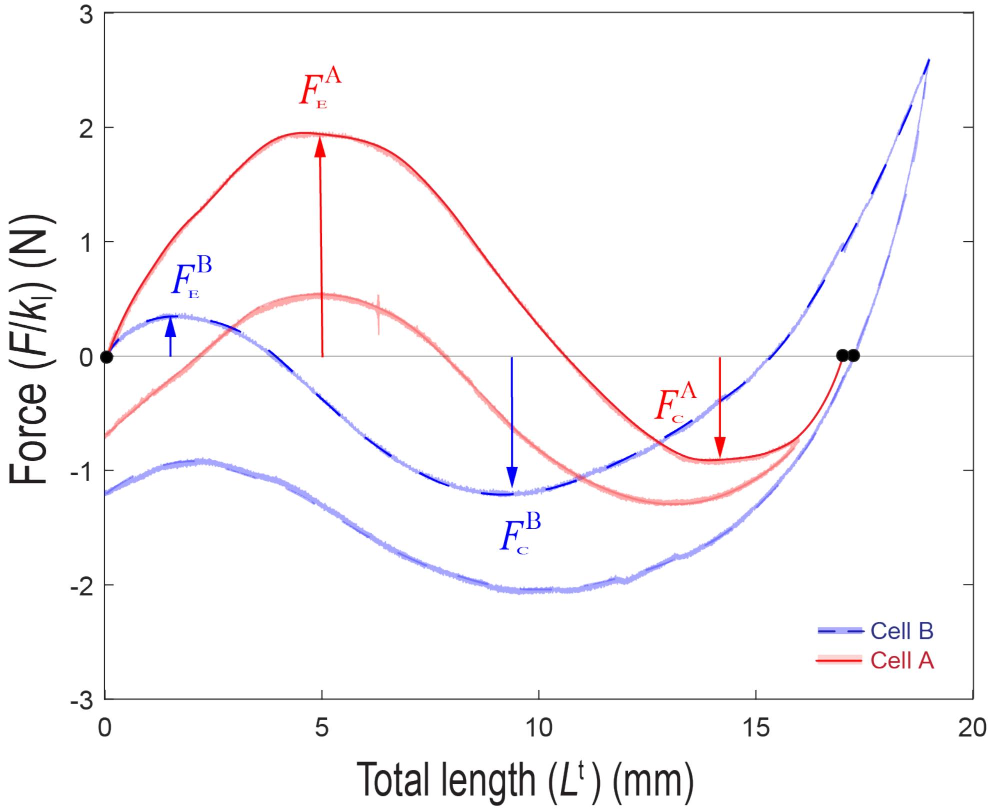

Figure 3.5: Measured force-displacement curves of the two unit cells prototype of the extension diode.

3.3 Conclusion

The only difference between the two sets (whether in "compression diode" or "extension diode") is the inter-cellular connection, one connected with the rod, and the other with the adhesive film along the zig-zag creases. This illustrates that the connection between two bi-stable cells can impose a kinematic constraint on the static behavior of the structure. In other words, the increase of critical force for shifting from one stable state to the next in the crease connection reveals the significant increase in the energy barrier in extending from '0-1' to '1-1' in extension diode setup and in compressing from '0-1' to '0-0' in compression diode.

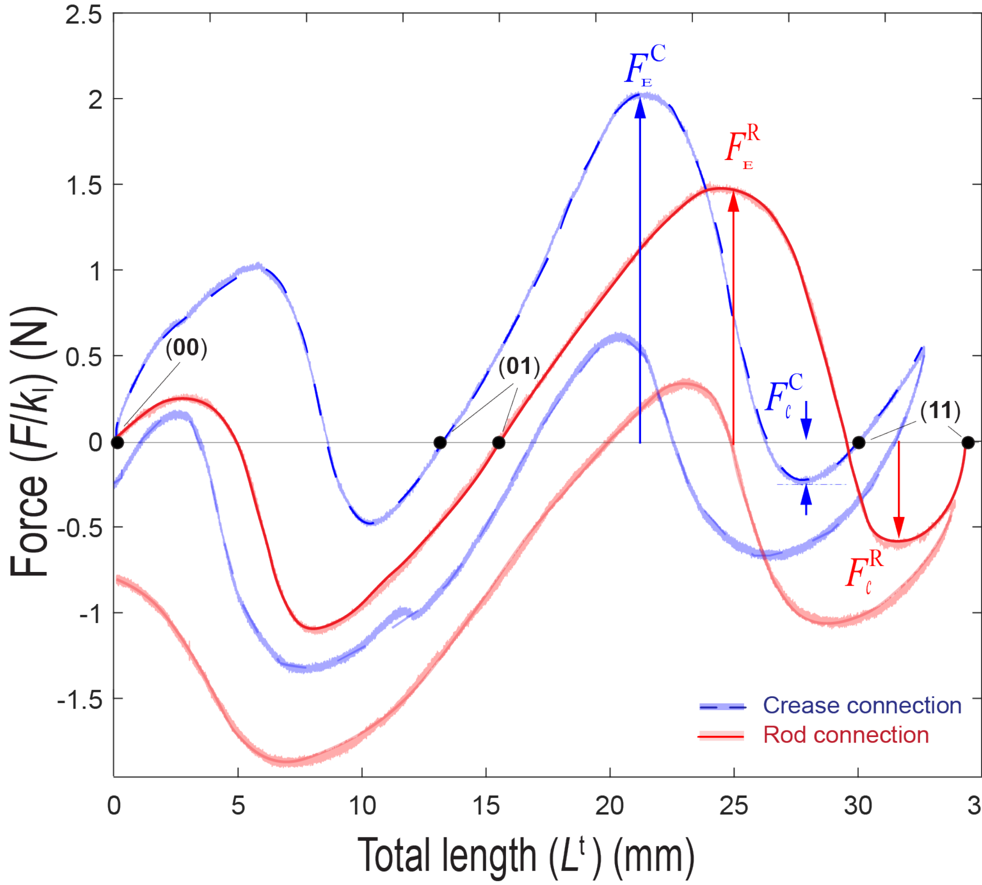

Figure 3.6: Tension and compression tests on extension diode dual-cell chain prototypes with rod connection (red curve) and crease connection (blue curve).

Observing the diode effect in these two dual cell chains (extension diode and compression diode) elucidates that this unique asymmetric energy barrier is the result of the coupling between unit cell length change in the z-axis and the connecting creases displacement along x and y axes at the boundary between two cells. This accentuates the importance of the three-dimensional nature of origami folding in obtaining mechanical diode behavior and multi-stability.

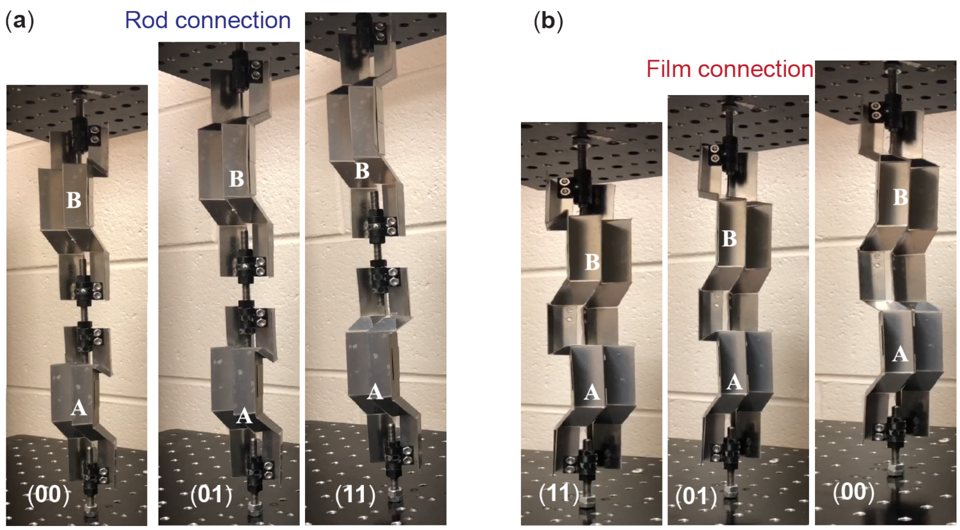

Figure 3.7: The photos of the rod-connected test (a) and crease-connected test of compression diode dual cell-chain (b) show the three stable states ('1-1','1-0', and '0-0')

Chapter 4

Optimization

4.1 Introduction

The primary objective of this study was to introduce a mechanical diode effect obtained by connecting two origami unit cells along their zigzag crease using adhesive film. Therefore, strengthening the diode effect is the prior concern in the design. On the other hand, minimizing the required material to fabricate a cellular structure is crucial to minimize the production cost. These two criteria were considered to find an optimum feasible solution region. The independent geometrical parameters were a_I,b_I,l_c, and γ_I). As it was mentioned in previous sections, the ideal diode behavior is originated from the nonlinearity in the describing correlations of the geometry. From the four involved parameters, γ_I is responsible for the biggest portion of the nonlinearity in the correlations describing the unit cell geometry (equations 2-7,...., 2-12).

The strength of the diode behavior can be measured by the ratio of the critical compression force to the extension force of the dual cell chain. The first objective is to maximize this ratio. The higher this ratio is, the stronger the mechanical diode can be achieved. In practice, the importance of this matter is revealed in the design of a mechanical logic gate to bear a high loading threshold.

Referring to previous sections, the derivative of the total stored elastic energy with respect to total length change gives the reaction force of the dual origami structure. Therefore, the design variables in the optimization process are the geometrical parameters used in potential energy evaluation including γ_I, a, b, and l_c.

To decrease the fabrication cost, the surface area of the unit cell should be minimized (note that the two cells are identical). The main constituents of the unit cell are: sheet I, sheet II and the connecting sheet.

Here, the inter-cellular connecting sheets are and the connectors that attach the two cells are assumed to have equal dimensions. The total surface area of the unit cell can be calculated as the summation of the areas of 4 parallelograms with sheet I dimensions and 4 parallelograms with sheet II dimensions and 2 rectangles with dimensions of the connecting sheet.

The total surface area is evaluated by the summation of the three following equations:

$$A_1 = 2a_I b_I \sin\gamma_I. \tag{4.1}$$

$$A_2 = 2a_{II} b_{II} \sin\gamma_{II}. \tag{4.2}$$

$$A_3 = 2b_I l_c. \tag{4.3}$$

4.2 Design problem

4.2.1 Design objective

The goal of this bi-objective optimization problem is to strengthen the diode behavior and at the same time to minimize the used material required for fabrication. In other words, the first objective is to maximize the defined force ratio and the second objective is minimizing the unit cell surface area. The next important step is to define all the geometrical constraints.

4.2.2 Design constraints

As it can be seen in figure 2-52.5, the unit cell poses the smallest length at $\theta_I = -90$. Therefore, it is important to take into consideration that the length of the inter-cellular connecting sheet is long enough to prevent any contact between sheet I and sheet II at this stable configuration. This geometrical constraint can be stated by the following inequality:

$$l_c > |l_I^{\max}| + |l_{II}^{\max}|\,. \tag{4.4}$$

Where l_I is the height of sheet one at $\theta_I = -90$ and l_{II} is the height of sheet II at the θ_{II} (2.3). LI and LII are calculated using following equations:

$$L_I = a_I \sin\theta_I \sin\gamma_I. \tag{4.5}$$

$$L_{II} = a_{II} \sin\theta_{II} \sin\gamma_{II}.. \tag{4.6}$$

4.2.3 Optimization problem setup

modeFrontier® 2017 R1 was used as the optimizer platform and MATLAB® 2017b was linked to the optimizer as the solver. DOE properties were adjusted at Basic mode with "Uniform Latin Hypercube" as the space filler. For this bi-criteria optimization problem "MOGA-II" method was used to carry out the optimization. "MOGA-II" which stands for "Multi-Objective Genetic Algorithm II" is an efficient evolutionary optimization algorithm for a constrained problem. Solving a multi-objective problem with the traditional form of the "Genetic Algorithm" can face deficiency in converging to the true "Pareto Front", and misidentify the true optima. "MOGA-II" algorithm tackles this issue with smart multi-search elitism. This new elitism operator has the advantage to preserve some desirable solutions without bringing the premature convergence into the local optimal fronts. In this method, the constraints are tackled by applying "Penalty Method", and it can handle both continuous and discrete design space (In the process of the optimization using this algorithm, the continuous design space is discretized internally) [37] . In modeFrotier®, the optimization algorithm configuration is set to the "automatic mode". In this configuration, The "Number of Generations" is 100, the "Probability of the Directional Cross-Over" is 0.5, the

"Probability of Mutation" is 0.1, the "DNA String Mutation Ratio" is 0.05, and the "Number of Evaluations" is chosen to be 2000 . The high values of the "Probability of Directional Cross-Over" decreases the robustness of the algorithm and this may cause the optimization process to get trapped at a local optima without touring the whole design space. This consideration matters in highly nonlinear problems, such as the "compression diode unit cell's geometry". Another important point is to enable the "Elitism" operator to enhance the convergence of the algorithm [37]. The workflow diagram can be seen in Figure 4.1.

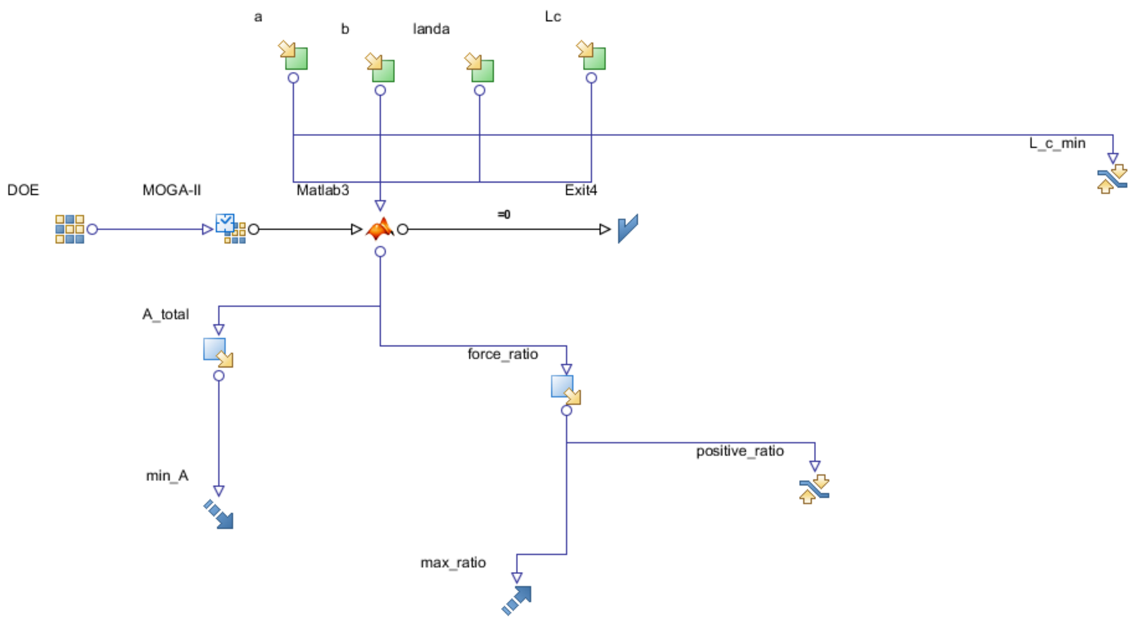

Figure 4.1: The developed workflow in modFrontier®to obtain optimized designs admissible region.

For a_I and b_I the lower bound of 0.5 cm and upper bound of 5 cm was chosen. γ_I varies between 45° and 75°, and l_c is changing from 0.8 cm to 5 cm. One should note that the different combinations of these design parameters can lead to mono-stability. Thus, it is crucial to allow only eligible designs into the optimization process. This constraint is defined in the MATLAB script linked to the optimizer.

4.3 Optimization results

Among the four design variables, γ_Il has a nonlinear relationship with angles defining the unit cell geometry; Therefore, the strength of the diode effect is highly sensitive to the variation of γ_I. More specifically, the spine angles, which quantify the kinematic constraint, are function of γ_I. This further demonstrates the impact of γ_I on the strength of the diode behavior of the structure. Sheet I and sheet II crease stiffnesses are function of a and b and the connecting sheet crease stiffness is a function of l_c. These stiffnesses have a linear relationship with the unit cell potential energy. These three design variables play a very important role in the surface area of the unit cell.

The obtained Pareto front from the optimizer is shown in Figure 4.2.

In the front, the force ratio varies from 18.5 to 36.9 and the surface area changes from 5.5 cm^2 to 17.3 cm^2. The design variables at the beginning of this range are $a_I = 0.5cm$, $b_I = 0.5cm$, $l_c = 1.1cm$, and $\gamma_I = 1.3rad$, and the at the end of the range are $a_I = 0.5cm$, $b_I = 1.8cm$, $l_c = 1.2cm$, and $\gamma_I = 1.3rad$ (Figure 4.3) . It is worth to note that γ_I value on the "Pareto Front" is consistently $1.3rad$. This shows that the optimum diode effect strength is achieved at this γ_I value and further illustrates the importance of this design parameter. However, parameter a_I value varies within the optimized designs range. Based on what type of application this structure is deployed in, and factors such as size and cost one objective can be the priority to the other one.

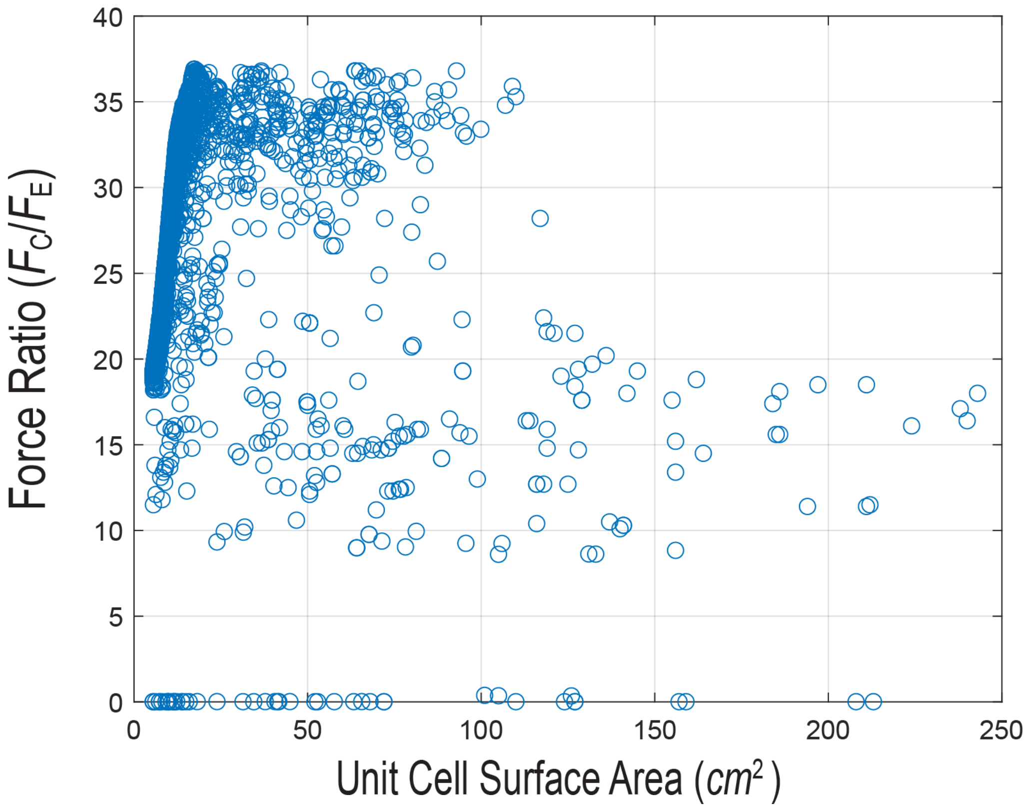

Figure 4.2: The"Pareto Front" for compression diode dual-cell chain.

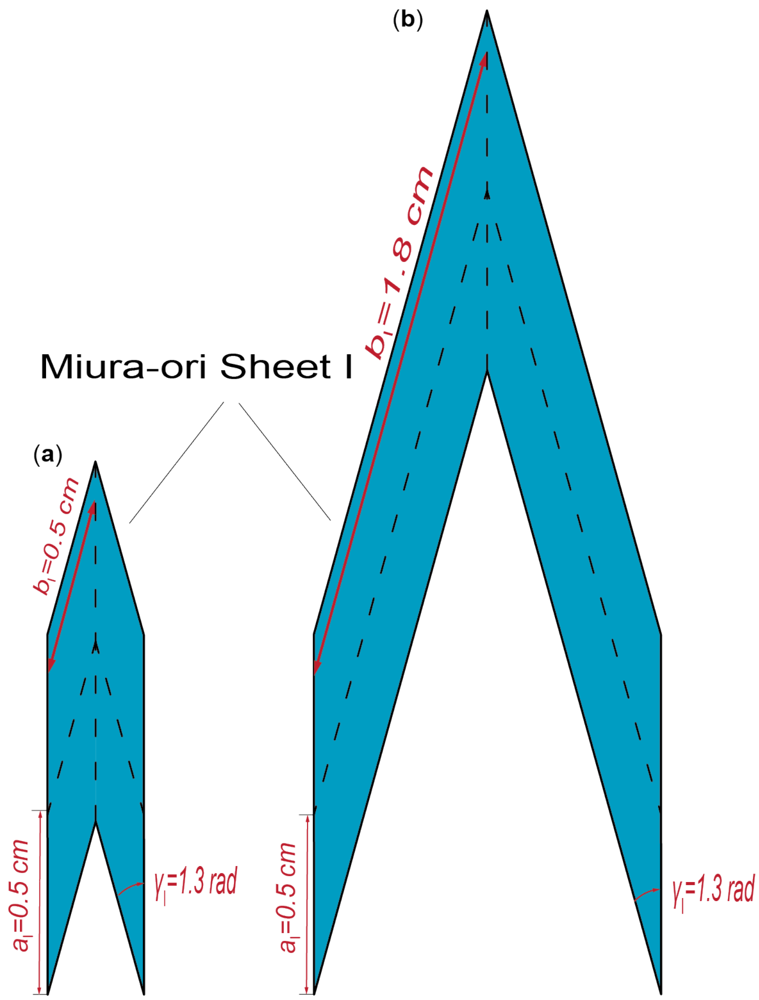

Figure 4.3: a) Miura-ori sheet I's geometry at the beginning of the optimum range. b) Miura-ori sheet I's geometry at the end of the optimum range.

Chapter 5

Conclusion and Future Work

5.1 Conclusion and Summary

This study proposes and examines a mechanics model to theoretically examine the static behavior of a multi-stable cellular origami structure that exhibits diode behavior in compression, presents experimental results to validate the theoretical results and, investigates, theoretically and experimentally, a transformed version of the compression diode unit cell that results in mechanical extension diode. Each unit cell in this cellular structure is essentially a bistable unit that consists of two geometrically consistent Miura-ori sheets and zig-zag shaped connecting sheet. The bi-stability in each cell originates from the nonlinear correlations between folding and crease deformation. It was shown that with a small change in the designed unit cell of the compression cellular structure, a new unit cell is obtained that shows diode behavior in extension. Each unit cell in this cellular structure is also a bi-stable unit that follows the same nonlinear correlation between the crease rotation and the overall folding.

The fundamental construction of this study was a dual-cell chain to investigate the static behavior of that. Using this dual-cell structure, the desired diode behavior was achieved in both compression and extension.

These origami unit cells (compression and extension diode designs) are essentially a three-dimensional transformation mechanism. This 3D nature of origami imposes a unique kinematic constraint onto the deformations of the two connected unit cells. More specifically, the magnitude mismatch between the spine angles of the two cells during deformation can determine the strength of the imposed kinematical constraint. This constraint can be quantified with an equivalent stiffness, k^*. The higher k^* results in a higher energy barrier either in compression direction or extension. In compression diode structure, due to this constraint, a higher force is required to deform the dual cell chain in compression direction while the required force to extend the structure is significantly smaller. In extension diode, the structure is easy to compress but hard to extend due to this added stiffness.

Then, two experimental setups were developed for both extension diode and compression diode to experimentally support the theoretical results. In the first set, the two unit cells are connected via a rigid rod with a balanced internal force. In the second setup, the two cells are connected via a zig-zag shaped connecting sheets along their zig-zag creases using adhesive film. The experimental observations revealed that the crease connection increases the energy barrier for switching between certain stable states. This increase for compression diode is in compressing the dual structure from one stable state to the next one and in the extension, it happens when the chain is being stretched from one stable state to the next.

Obtaining diode-like behavior by employing nonlinear elastic properties to achieve diode-like mechanical behavior is a progressively important subject of research [9]. In recent studies, it has been shown that multi-stable structures and materials with carefully designed microstructures are capable of attaining unidirectional acoustic [2] and elastic wave propagation [34]. The diode effect reported in this study can open new avenues toward multifunctional structures and material systems that can be deployed in motion rectifying, wave propagation control, and mechanical computation.

5.2 Future Work

In chapter 3, a notable hysteresis was observed in the experimental force-displacement curves. This hysteresis was due the plastic deformation of "Adhesive UHMW Polyethylene Film" during the full loading cycle. If one runs the experiment for more than one cycle, the second or third cycle does not result in desirable F_D curves and the multi-stability behavior can not be concluded from the second or third loading cycles graphs. Thus, it is important to find an alternative to assemble the structure that can address the hysteresis issue and enhance the experiment repeatability. Moreover, the magnitude of increased forced between rod connection and crease connection (the increase in the tension reaction force in extension diode and increase in the compression reaction force in compression diode) was expected to be higher. One improvement in the experimental setup should be strengthening the crease connection between two unit cells.

Developing a finite element model of the unit cell, and the stacked cellular structure is a very efficient tool to further investigate the mechanics of the developed theoretical model. This FEA model can be used to do a stress analysis on the static diodes and study the kinematics of the structure. Moreover, based on the results of these studies one can apply required modifications to further enhance the unit cells design and performance according to the anticipsted application. Additionally, developing a logic gate based on these two unit cells is the next phase of this project to demonstrate the capabilities of these designs in practice.

Appendix A

Prototype Fabrication Process

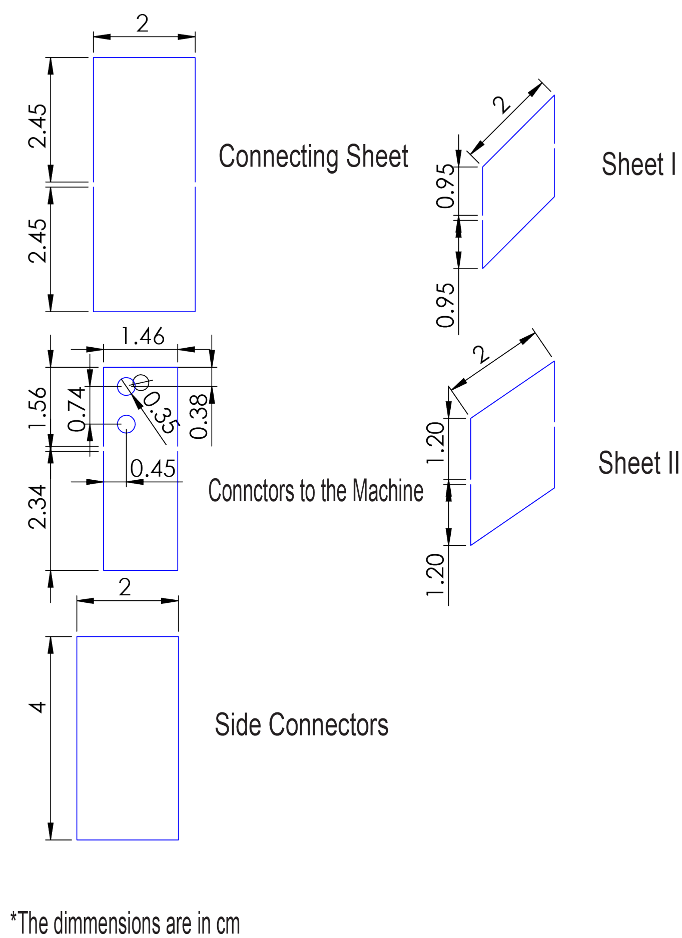

Figure A.1: SolidWork drawings of the fabricated prototype

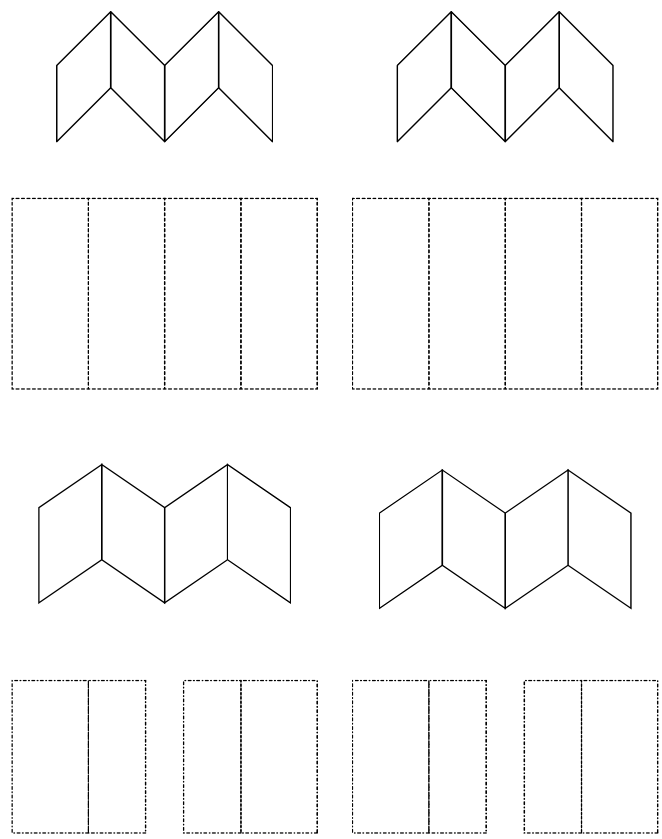

Figure A.2: The used outlines of the subsets that are connected to each to assemble the dual structure using the method introduced in Appendix A

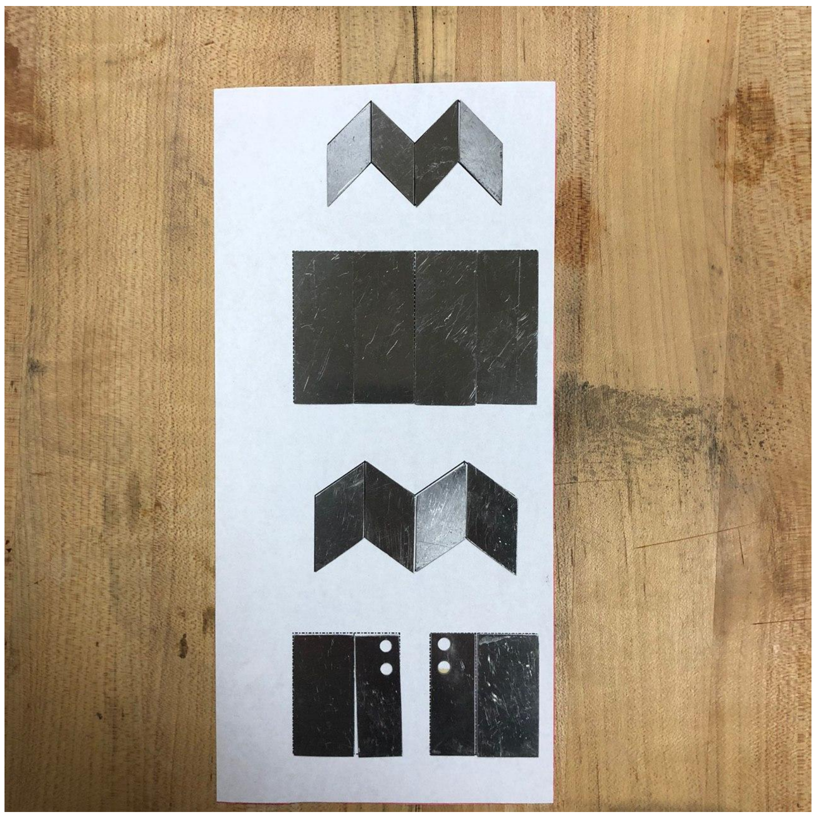

Figure A.3: Step 1. The cut parts should be fixed on the proper place on the outline as shown in Figure A.3

Figure A.4: Step 2.

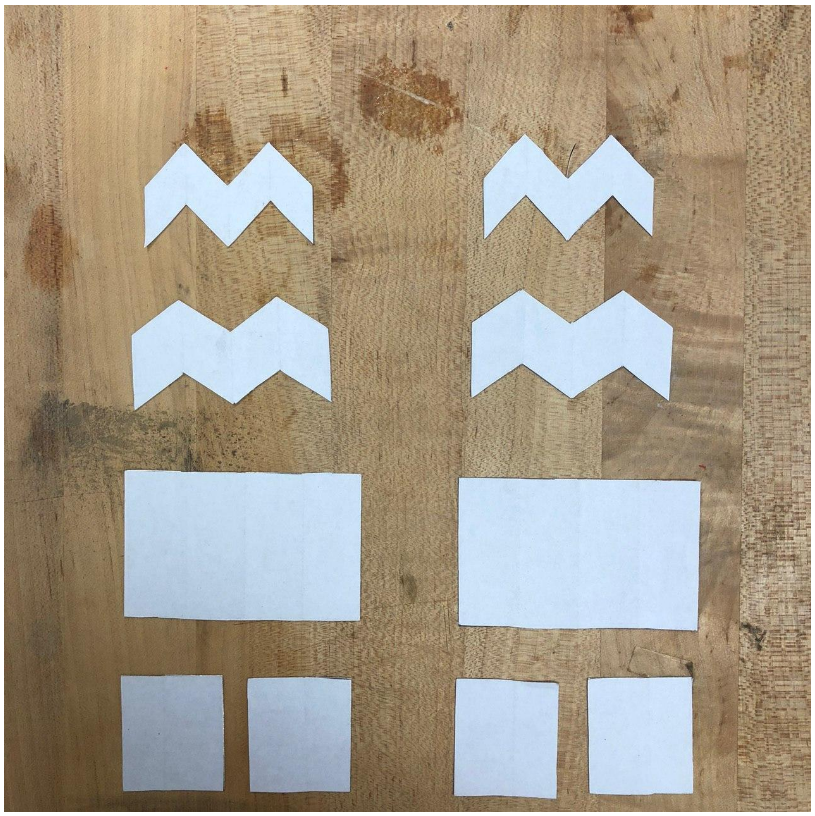

Figure A.5: Step 3.

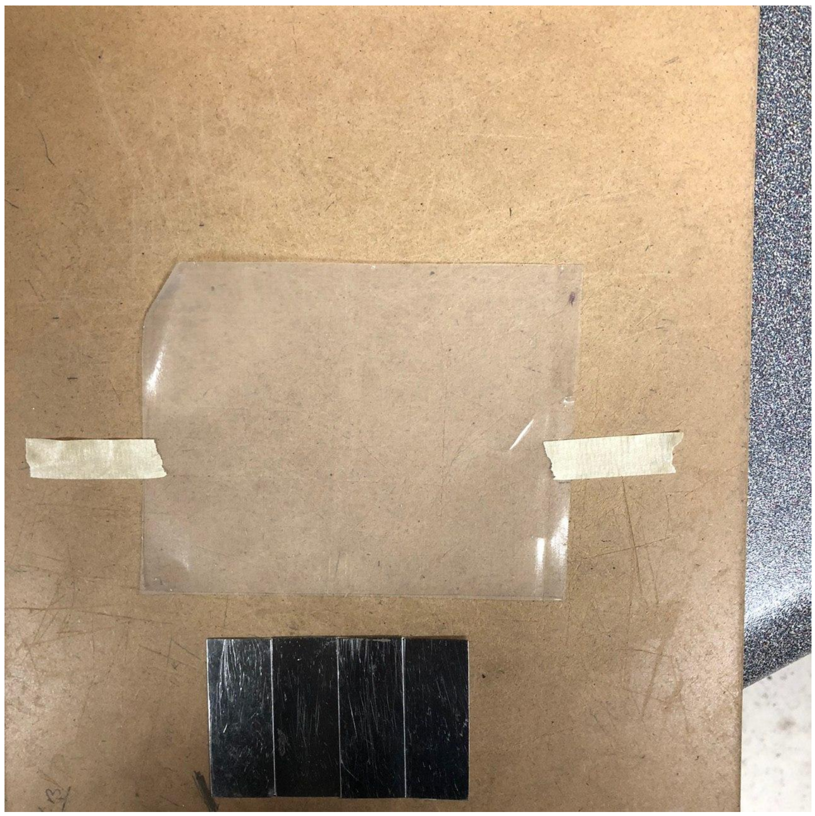

Figure A.6: Step 4: Fixing a piece of adhesive film with the sticky side facing upward.

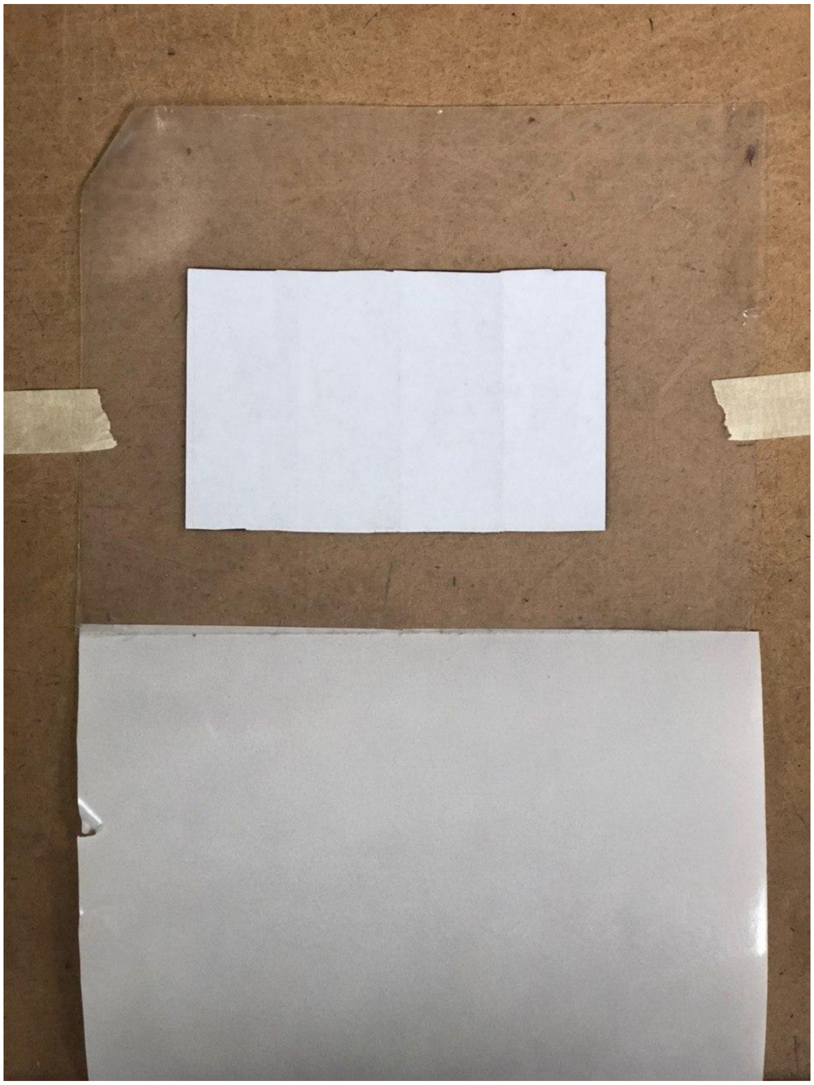

Figure A.7: Step 5: The ”slippery sheet” should be kept to be used in next step.

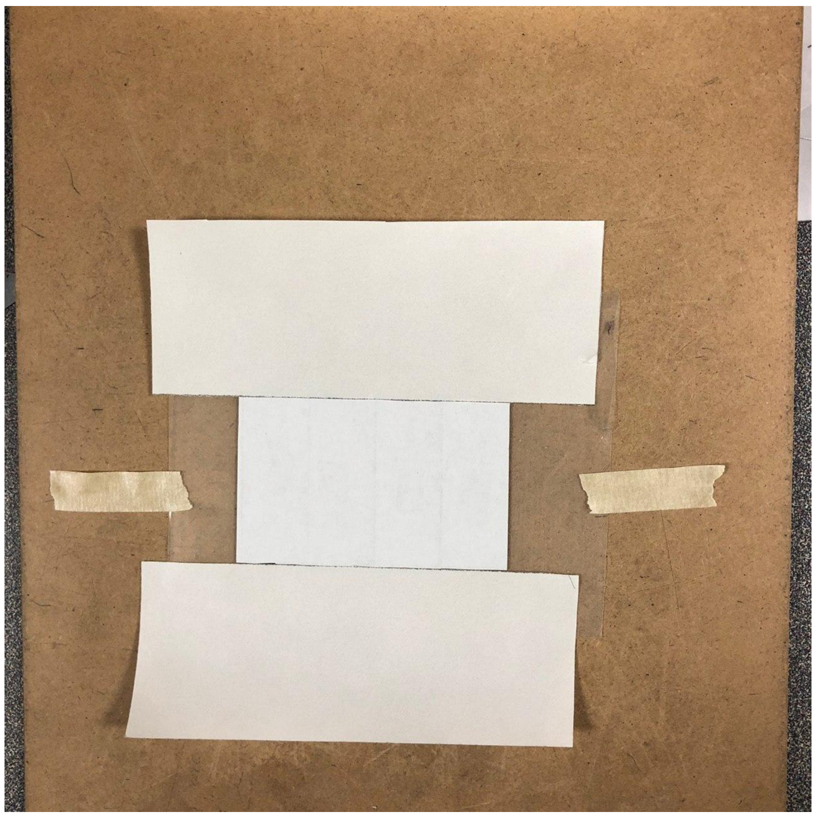

Figure A.8: Step 6: Attache the "slippery sheet" as it shown in the figure form the slippery side to the adhesive film.

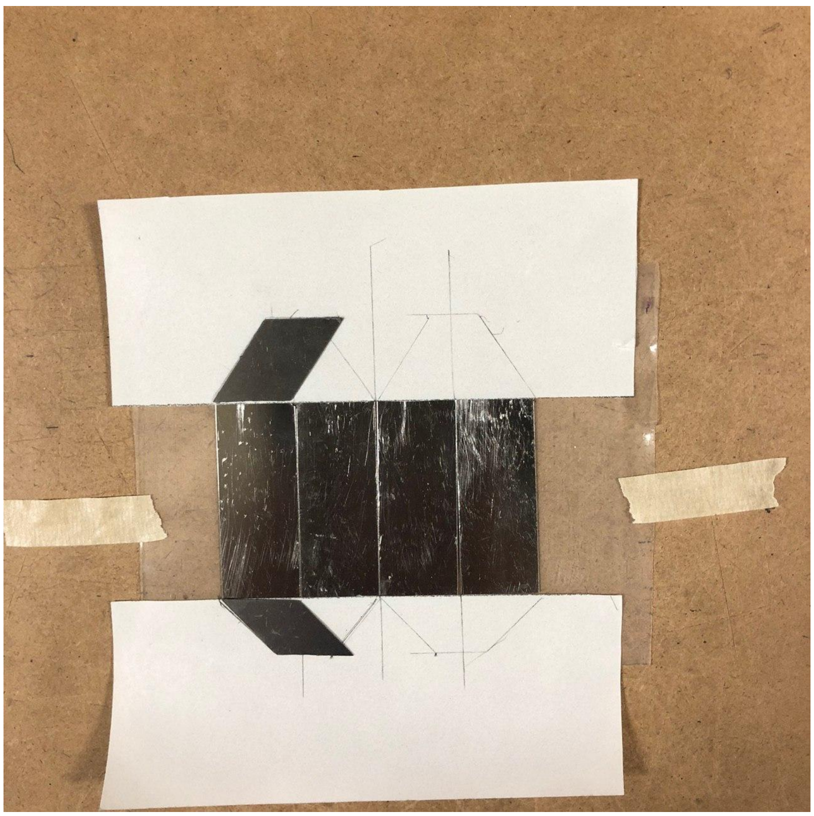

Figure A.9: Step 7. Drawing the flaps of the connecting sheets using the sheet I and sheet II parallelograms.

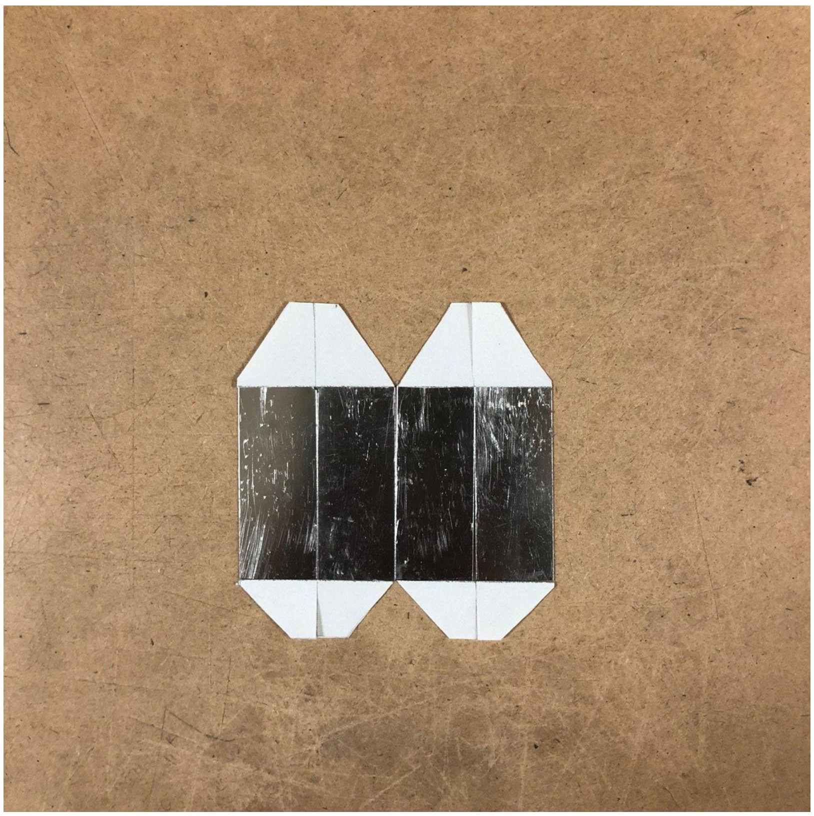

Figure A.10: Step 8

Figure A.11: Step 9

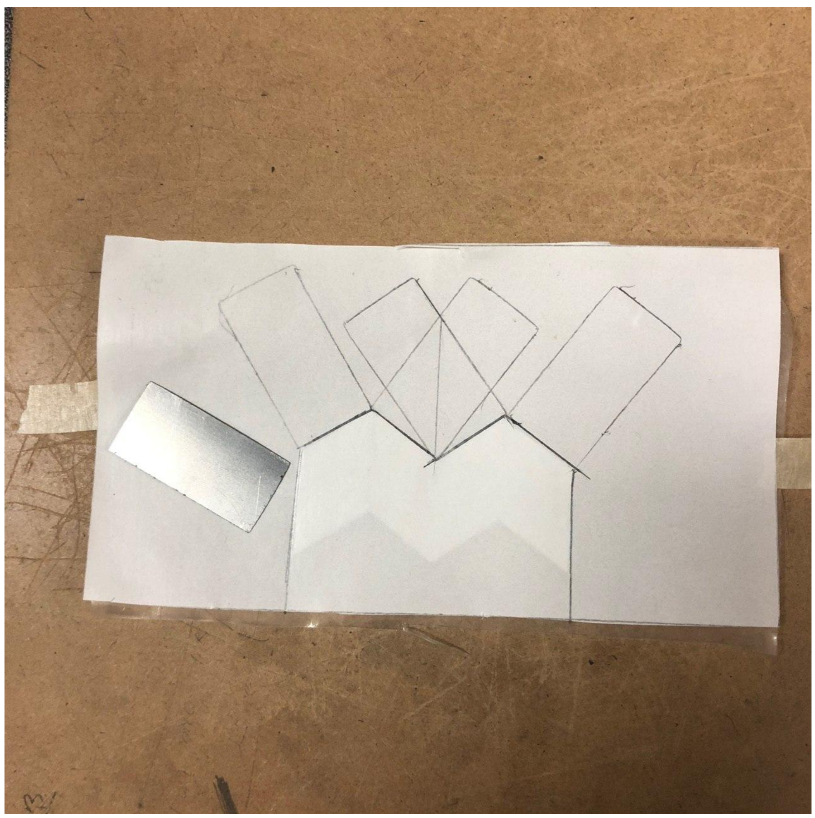

Figure A.12: Step 10. Drawing the flaps of the sheet I using the side connecting sheet part.

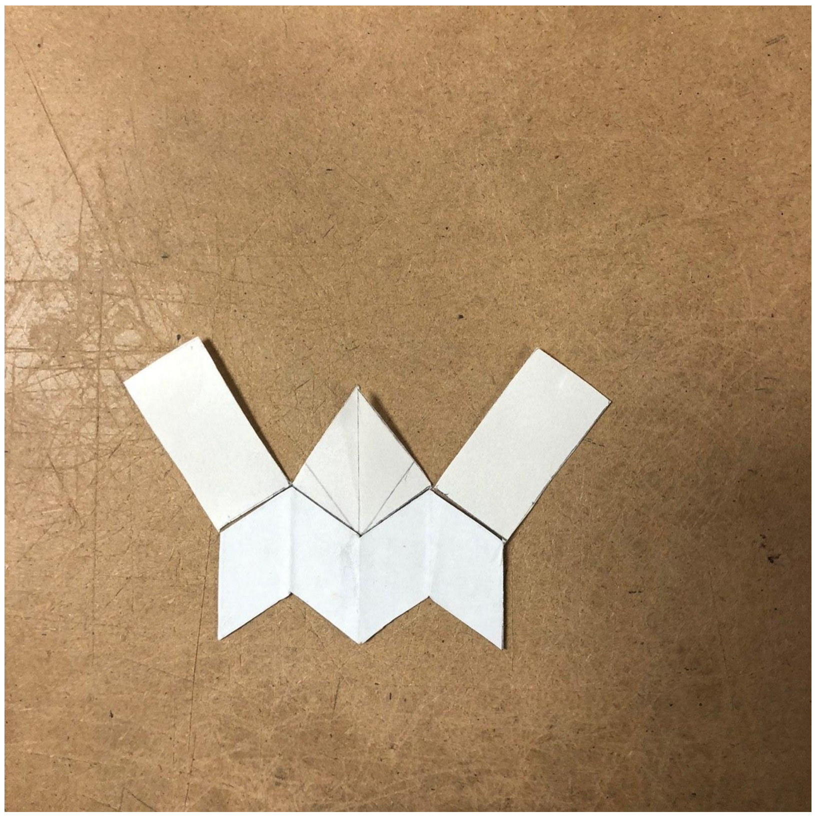

Figure A.13: Step 11

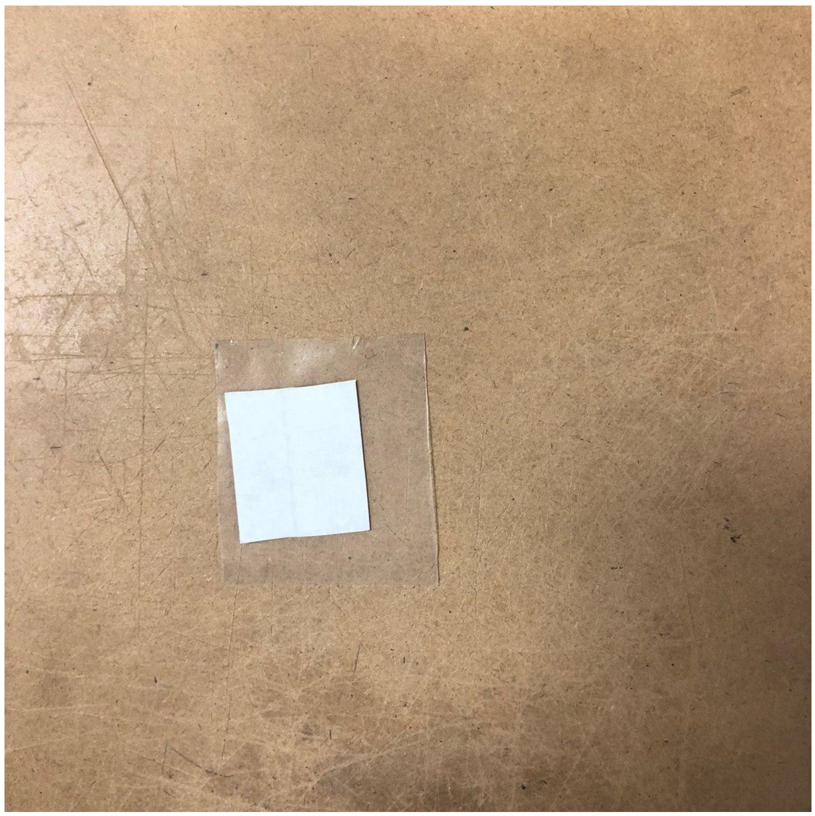

Figure A.14: Step 12

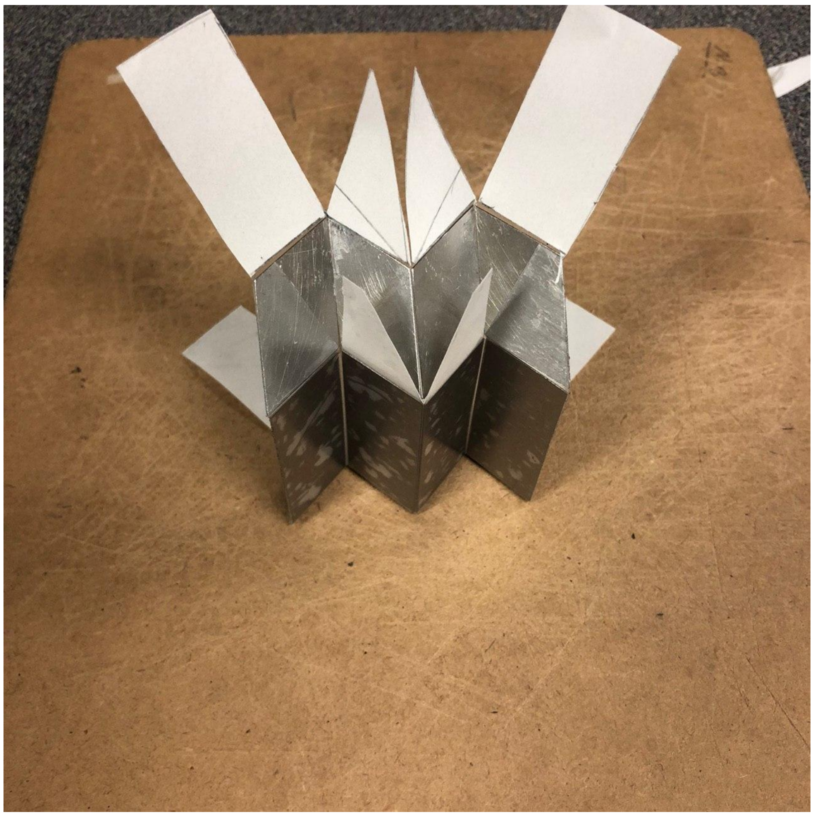

Figure A.15: Step 13. Attaching the subsets to eaxh other along their flaps.

Figure A.16: Step 14.

Appendix B

MATLAB®Codes

B.1 Theoretical Analysis Main MATLAB Script for $k^* = 50$ Compression Diode

```
clear
clc
clf
close all
%%CELL A parameters
aIa=2;
% bIa=aIa;
bIa=4;
aIIa=1.25*aIa;
landaIa=pi/4;
landaIIa=acos((aIa*cos(landaIa))/aIIa); % rigid-folding condition
KIa=1;
K_A=zeros(1,5);
```

```
K_A(1,1)=KIa;
L_c=5;
L_o=5;
theta0_a=-pi/3;
theta_a1_2_0=acos((cos(theta0_a).*tan(landaIa))./(tan(landaIIa)));

K_A(1,2)=20*KIa;
K_A(1,3)=KIa;
K_A(1,4)=KIa;
K_A(1,5)=0;
theta_a1=linspace(-pi/2,pi/2,1555);
theta_a1_2=acos((cos(theta_a1).*tan(landaIa))./(tan(landaIIa)));
theta_a1_2_0=acos((cos(theta0_a).*tan(landaIa))./(tan(landaIIa)));
s1a=sin(landaIa);
t2a=tan(landaIIa);
t1a=tan(landaIa);
L1_a=aIa.*sin(theta_a1).*sin(landaIa);
L2_a=aIIa.*sin(theta_a1_2).*sin(landaIIa);
n=length(L1_a);
L2_a_max=max(L2_a);
L1_a_max=max(L1_a);
L2_a_min=min(L2_a);
L1_a_min=min(L1_a);
LA_min=L2_a_min+L1_a_min+L_c;
LA_max=L2_a_max+L1_a_max+L_c;
% LA=linspace(LA_min,LA_max,n);
LA_I=linspace(L1_a_min,L1_a_max,length(L1_a)); %length of sheet I in new
    design

%%
%%CELL B parameters
```

```
aIb=2;
bIb=aIb;
aIIb=1.25*aIb;
landaIb=pi/4;
landaIIb=acos((aIb*cos(landaIb))/aIIb); % rigid-folding condition
KIb=1;
K_B=zeros(1,5);
K_B(1,1)=KIb;

theta0_b=pi/3;
theta_b2_0=acos((cos(theta0_b).*tan(landaIb))./(tan(landaIIb)));

K_B(1,2)=20*KIb;
K_B(1,3)=KIb;
K_B(1,4)=KIb;
K_B(1,5)=0;
theta_b1=linspace(-pi/2,pi/2,n);
theta_b2=acos((cos(theta_b1).*tan(landaIb))./(tan(landaIIb)));
s1b=sin(landaIb);
t2b=tan(landaIIb);
t1b=tan(landaIb);
L1_b=aIb.*sin(theta_b1).*sin(landaIb);
L2_b=aIIb.*sin(theta_b2).*sin(landaIIb);
L_b=L_c+L1_b-L2_b;
L2_b_max=max(L2_b);
L1_b_max=max(L1_b);
L2_b_min=min(L2_b);
L1_b_min=min(L1_b);
%%
%Total length CEll A_I_II in  original design
A=aIa*sin(landaIa);
```

```
B=((tan(landaIIa))^2)/((tan(landaIa))^2);


L_a=aIa*s1a*((sqrt(((t2a^2)/(t1a^2))-((cos(theta_a1).^2))))-sin(theta_a1
    ));
L_A_max=max(L_a)
L_A_min=min(L_a)
%%
%Mismatch parameters
K_star=50;

say_A0=2*atan(cos(theta0_a)*tan(landaIa));
say_B0=2*atan(cos(theta0_b)*tan(landaIb));

n=length(L1_a)
%%


%%
%Calculating maximum and minium
i5=0;
for i3=linspace(-pi/2,pi/2,n)

    i5=i5+1;
    i6=0;
    for i4=linspace(-pi/2,pi/2,n)
        i6=i6+1;
        theta_a1_2(i5)=acos((cos(i3).*tan(landaIa))./(tan(landaIIa)));
        theta_b_2(i6)=acos((cos(i4).*tan(landaIb))./(tan(landaIIb)));
        total_length(i5,i6)=(L_c+(aIa.*sin(i3).*sin(landaIa))-abs((aIIa
            .*sin(theta_a1_2(i5)).*sin(landaIIa))))+(L_c+(aIb.*sin(i4).*
```

```
sin(landaIb))-abs((aIIb.*sin(theta_b_2(i6)).*sin(landaIIb)))
    )+L_o;
    end

end
L_total_min=min(min(total_length));
L_total_max=max(max(total_length));
L_T=linspace(L_total_min,L_total_max,n); %New design total length
%%

i1=0;
for LT=linspace(L_total_min,L_total_max,n)
    i1=i1+1;
  for i2=1:length(L1_a)
        [theta_A1(i1,i2),theta_A2(i1,i2),E_A(i1,i2),LA_II(i1,i2),
            L_A_I_II(i1,i2)]=CellA(LA_I(i2),landaIa,aIa,bIa,K_A,theta0_a
            ,n,L_o,L_c);
        [E_B(i1,i2),LB_I_II(i1,i2),theta_B(i1,i2),E1_b2(i1,i2),E2_b2(i1,
            i2),E3_b2(i1,i2),E4_b2(i1,i2),E7_b2(i1,i2)]= CellB(aIb,aIIb,
            landaIb,LA_I(i2),LA_II(i1,i2),K_B,theta0_b,L2_a_min,L2_a_max
            ,L_A_I_II(i1,i2),n,LT,L_o,L_c);
        if E_B(i1,i2)~=0
            say_A(i1,i2)=2*atan((cos(theta_A1(i1,i2)))*tan(landaIa));
            say_B(i1,i2)=2*atan((cos(theta_B(i1,i2)))*tan(landaIb));
            E_say(i1,i2)=K_star*bIa*(((say_A(i1,i2)-say_B(i1,i2)).^2)./2)
                ;
            E6_a2(i1,i2)=(K_A(3).*(say_A(i1,i2)-say_A0).^2)./2;
            E6_b2(i1,i2)=(K_B(3).*(say_B(i1,i2)-say_B0).^2)./2;
            E8_A_B(i1,i2)=(K_A(5).*(say_B(i1,i2)-say_A(i1,i2)).^2)./2;

            Et_A_B(i1,i2)=E_A(i1,i2)+E_B(i1,i2);
```

```
            Et_say(i1,i2)=Et_A_B(i1,i2)+E_say(i1,i2)+E8_A_B(i1,i2)+E6_a2(
                i1,i2)+E6_b2(i1,i2);
        else
            say_A(i1,i2)=0;
            say_B(i1,i2)=0;
            E_say(i1,i2)=0;
            E6_a2(i1,i2)=0;
            E6_b2(i1,i2)=0;
            E8_A_B(i1,i2)=0;
            Et_A_B(i1,i2)=0;
            Et_say(i1,i2)=0;

        end
    end
end

%%
%
% %Plotting results
for i=1:n
    L1_a_2(i)=aIa.*sin(theta_A1(1,i)).*sin(landaIa);
    L2_a_2(i)=aIIa.*sin(theta_A2(1,i)).*sin(landaIIa);
    LA(i)=L1_a_2(i)-L2_a_2(i)+L_c;
end

[X1,Y1]=meshgrid(L_T,LA);
XX1=X1.';
YY1=Y1.';
% %%
% %Total energy
% figure(1)
```

```
% V1=linspace(0,1000,100); %energy level
%
% contourf(XX1,YY1,Et_say)
% xlabel('Total Length')
% ylabel('Cell A_Sheet I length')
% title('Total Energy Contour')
%
% %%
% %Thet_A1
% figure(2)
% plot3(XX1,YY1,theta_A1)
% title('Theta_A_I')
% %%
% %Theta_A2
% figure(3)
% plot3(XX1,YY1,theta_A2)
% title('Theta_A_II')
% %%
% %Theta_B
% figure(4)
% plot3(XX1,YY1,theta_B)
% title('Theta_B')
% %%
%
% %plotting energy landscape of cell A
% theta_A1_2=linspace(-pi/2,pi/2,n);
% % L_A_I_II_2=abs(aIa*s1a*((sqrt(((t2a^2)/(t1a^2))-((cos(theta_A1_2)
    .^2))))-sin(theta_A1_2)));
% L1_A_I_2=aIa.*sin(theta_A1_2).*sin(landaIa);
% phi10_a=pi-2.*theta0_a;
% phi20_a=2.*asin(cos(theta0_a)./sqrt(1-((sin(theta0_a)).^2).*(sin(
```

```
landaIa)).^2)); %it should not be more than 1 or -1
% phi30_a=pi-(2.*acos(tan(landaIa).*(1/(tan(landaIIa))).*cos(theta0_a)));
% phi40_a=2.*asin(((sin(landaIa))./(sin(landaIIa))).*sin(phi20_a./2));
% phi50_a=(pi/2)+theta0_a  ;  %it should not be more than 1 or -1
% s1a=sin(landaIa);
% t2a=tan(landaIIa);
% t1a=tan(landaIa);
% phi1_a1=pi-2.*theta_A1_2;
% phi2_a1=2.*asin(cos(theta_A1_2)./sqrt(1-((sin(theta_A1_2)).^2).*(sin(landaIa)).^2));
% phi3_a1=pi-(2.*acos(tan(landaIa).*(1/(tan(landaIIa))).*cos(theta_A1_2)));
% phi4_a1=2.*asin(((sin(landaIa))./(sin(landaIIa))).*sin(phi2_a1./2));
% phi5_a1=(pi/2)+theta_A1_2;
% say_A1_2=2*atan(cos(theta_A1_2)*tan(landaIa));
% say_A1_2_0=2*atan(cos(theta0_a)*tan(landaIa));
% K1_a=2*K_A(1)*bIa;  %KIa
% K2_a=2*K_A(1)*aIa;  %KIa
% K3_a=2*K_A(2)*bIa;  %KIIa
% K4_a=2*K_A(2)*aIIa; %KIIa
% K6_a=2*L_c*K_A(3); %inter celllar crease stiffness . there are tow creases with theire associated stiffness in each unit cell
%                        %Kc3_a
% K7_a=8.*K_A(4).*bIa; %Kc2_a
% K8_a=K_A(5).*bIa; %K_external
% E1_a1=K1_a.*(phi1_a1-phi10_a).^2;
% E2_a1=K2_a.*(phi2_a1-phi20_a).^2;
% E3_a1=K3_a.*(phi3_a1-phi30_a).^2;
% E4_a1=K4_a.*(phi4_a1-phi40_a).^2;
% E6_a1=K6_a.*(say_A1_2-say_A1_2_0).^2;
```

```
% E7_a1=K7_a.*(phi5_a1-phi50_a).^2;
% Et_a=(E1_a1+E2_a1+E3_a1+E4_a1+E7_a1+E6_a1+E7_a1)./2;
% figure(5)
% plot(L1_A_I_2,Et_a)
% %%
% %Eenrgy lanscape
% figure(6)
% plot3(XX1,YY1,Et_say)
% title('Total energy Landscape')
% %%
% %Plotting CELL B energy landscape
% figure(7)
% plot3(XX1,YY1,E_B)
% title('Cll B energy Landscape')
% %%
% %Plotting CELL B energy landscape
% figure(8)
% plot3(XX1,YY1,E_A)
% title('Cll A energy Landscape')
% %%
% % Kinematic Constraint  Energy Contour
% V2=linspace(0,100,100); %energy level
% figure(9)
% contour(XX1,YY1,real(E_say),V2)
% xlabel('Total Length')
% ylabel('Cell A_Sheet I length')
% title('Kinematic Constraint  Energy Contour')
% %%
% %Plotting total energy contour with total length of cell A on y axis
%
% LA1_min=L2_a_min+L1_a_min+L_c;
```

```
% LA1_max=L2_a_max+L1_a_max+L_c;
% LA1_range=linspace(LA1_min,LA1_max,n);
% [X2,Y2]=meshgrid(L_T,LA1_range);
% XX2=X2.';
% YY2=Y2.';
% figure(10)
% contour(XX2,YY2,real(E_say),V2)
% xlabel('Total Length')
% ylabel('Cell A length')
% title('Total Energy Contour')
%
% %%
% %Plotting say
% figure(18)
% plot3(XX1,YY1,say_A)
% title('Say_A')
% %%
% figure(19)
% plot3(XX1,YY1,say_B)
% title('Say_B')
%
% %%
% %Plotting E_say
% figure(20)
% plot3(XX1,YY1,E_say)
% title('ESay')
% %%
% %Plotting E8_A_B
% figure(21)
% plot3(XX1,YY1,E8_A_B)
% title('E8_A_B')
```

```
% %%
% %Plotting  E6_a2
% figure(22)
% plot3(XX1,YY1,E6_a2)
% title('E6_a2')
%
% %%
% %Plotting  E6_b2
% figure(23)
% plot3(XX1,YY1,E6_b2)
% title('E6_b2')


 figure(24)


Maxima=[];
Index=[];
Index2=[];
Index3=[];
Index4=[];
Minima1=[];
Minima2=[];
Minima3=[];
Minima4=[];
Index4=[];
Index5=[];
satreMinima1=[];
satreMinima2=[];
satreMinima3=[];
satreMinima4=[];
```

```
sotooneMinima1=[];
sotooneMinima2=[];
sotooneMinima3=[];
sotooneMinima4=[];
satreMaxima=[];
Maxima8=[];
satreMaxima8=[];
Index8=[];
first_false_maxima=[];

Minima11=[];
Minima22=[];

Index22=[];
satreMaxima2=[];
Maxima2=[];
for z1=1:n

    if z1<=40
        [maxima,index1]=max(Et_say(z1,:));
        Maxima=[Maxima maxima];
        satreMaxima=[satreMaxima z1];
        Index=[Index index1];
    elseif z1<=1400
        aaaaa=sum(Et_say(z1,:)>0);
        if Et_say(z1,n)==0
            [maxima,index1]=max(Et_say(z1,floor(aaaaa*0.2):aaaaa-floor(aaaaa*0.4)));
            index1=index1+floor(aaaaa*0.2)-1;
            Maxima=[Maxima maxima];
            satreMaxima=[satreMaxima z1];
```

```
            Index=[Index index1];
        elseif Et_say(z1,1)==0
            [maxima index1]=max(Et_say(z1,n-aaaaa+floor(aaaaa*0.2):n-
                floor(aaaaa*0.2)));
            index1=index1+n-aaaaa+floor(aaaaa*0.2)-1;
            Maxima=[Maxima maxima];
            satreMaxima=[satreMaxima z1];
            Index=[Index index1];
        else
            [maxima index1]=max(Et_say(z1,30:995));
            index1=index1+29
            Maxima=[Maxima maxima];
            satreMaxima=[satreMaxima z1];
            Index=[Index index1];

        end
    else
        [maxima index1]=max(Et_say(z1,:));
        Maxima=[Maxima maxima];
        satreMaxima=[satreMaxima z1];
        Index=[Index index1];
    end


    minima1=maxima;
    minima2=maxima;
    index2=[];
    index3=[];
    for ii=1:index1-1
        if Et_say(z1,ii)>0
            if minima1>Et_say(z1,ii)
```

```
                minima1=Et_say(z1,ii);
                index2=ii;
            end
        end
    end
    index4=ii;

    for ii=index1+1:n
        if Et_say(z1,ii)>0
            if minima2>Et_say(z1,ii)
                minima2=Et_say(z1,ii);
                index3=ii;
            end
        end
    end

    if abs(minima1-maxima)>1e-6
        Minima1=[Minima1 minima1];
        Minima11=[Minima11 minima1];
        satreMinima1=[satreMinima1 z1];
        sotooneMinima1=[sotooneMinima1 index2];
    else

          minima1=0;
          Minima11=[Minima11 minima1];
    end

    if abs(minima2-maxima)>1e-6
        Minima2=[Minima2 minima2];
        Minima22=[Minima22 minima2];
        satreMinima2=[satreMinima2 z1];
```

```
            sotooneMinima2=[sotooneMinima2  index3];
      else

                minima2=0;
                Minima22=[Minima22  minima2];
      end
end
%%
%after finding the minuimums and maximums , i need to plot the valuse vs
%tital length and length of A
L1X=[];
L1Y=[];
z8=0;
for z7=1:length(sotooneMinima1)
      z8=z8+1;
      l1x=XX1(satreMinima1(z8),sotooneMinima1(z7));
      L1X=[L1X  l1x];
      l1y=YY1(satreMinima1(z8),sotooneMinima1(z7));
      L1Y=[L1Y  l1y];

end

L2X=[];
L2Y=[];
z10=0;
for z9=1:length(sotooneMinima2)
      z10=z10+1;
      l2x=XX1(satreMinima2(z10),sotooneMinima2(z9));
      L2X=[L2X  l2x];
      l2y=YY1(satreMinima2(z10),sotooneMinima2(z9));
      L2Y=[L2Y  l2y];
```

```
end


L4X=[];
L4Y=[];
z13=0;

for z14=1:length(Maxima)
      z13=z13+1;
      l4x=XX1(satreMaxima(z13),Index(z14));
      L4X=[L4X l4x];
      l4y=YY1(satreMaxima(z13),Index(z14));
      L4Y=[L4Y l4y];

end

L4X2=[];
L4Y2=[];
z132=0;

for z14=1:length(Maxima2)
      l4x=XX1(satreMaxima2(z14),Index22(z14));
      L4X2=[L4X2 l4x];
      l4y=YY1(satreMaxima2(z14),Index22(z14));
      L4Y2=[L4Y2 l4y];
end
```

```
hold on

for i=1:30
    hold on
    LT=XX1(780+i,:);
    LA=YY1(780+i,:);
    ZZZ3=Et_say(780+i,:);
    plot3(LT,LA,ZZZ3)
end

% plot3(XX1,YY1,Et_say)
% colormap('pink')
plot3(L1X,L1Y,Minima1,'or')
plot3(L2X,L2Y,Minima2,'og')
plot3(L4X,L4Y,Maxima,'oc')

bbbb=length(L4X)-sum((L4X>10.5))
dddd=sum((L4X<12.8))

plot3(L4X(bbbb:dddd),L4Y(bbbb:dddd),Maxima(bbbb:dddd),'oc')

axis([L_T(1) L_T(n) LA(1) LA(n)])
set(gca,'XTick',[], 'YTick', [])
% plot3(L4X,L4Y,Maxima,'oc')

% plot3(L4X2,L4Y2,Maxima2,'oy')


%%

```

```
%Computing enregy derivative

Maxima=[];
Index=[];
Index2=[];
Index3=[];
Index4=[];
Minima1=[];
Minima2=[];
Minima3=[];
Minima4=[];
Index4=[];
Index5=[];
satreMinima1=[];
satreMinima2=[];
satreMinima3=[];
satreMinima4=[];
sotooneMinima1=[];
sotooneMinima2=[];
sotooneMinima3=[];
sotooneMinima4=[];
satreMaxima=[];
Maxima8=[];
satreMaxima8=[];
Index8=[];
first_false_maxima=[];

Minima11=[];
Minima22=[];
```

```
Index22=[];
satreMaxima2=[];
Maxima2=[];

for z1=1:n


    if z1<=4000000000
        [maxima,index1]=max(Et_say(z1,:));
        Maxima=[Maxima maxima];
        satreMaxima=[satreMaxima z1];
        Index=[Index index1];
    elseif z1<=1545
        aaaaa=sum(Et_say(z1,:)>0);
        if Et_say(z1,999)==0
            [maxima,index1]=max(Et_say(z1,floor(aaaaa*0.2):aaaaa-floor(aaaaa*0.4)));
            index1=index1+floor(aaaaa*0.2)-1;
            Maxima=[Maxima maxima];
            satreMaxima=[satreMaxima z1];
            Index=[Index index1];
        elseif Et_say(z1,1)==0
            [maxima index1]=max(Et_say(z1,n-aaaaa+floor(aaaaa*0.2):n-floor(aaaaa*0.2)));
            index1=index1+n-aaaaa+floor(aaaaa*0.2)-1;
            Maxima=[Maxima maxima];
            satreMaxima=[satreMaxima z1];
            Index=[Index index1];
        else
            [maxima index1]=max(Et_say(z1,30:995));
            index1=index1+29
```

```
            Maxima=[Maxima maxima];
            satreMaxima=[satreMaxima z1];
            Index=[Index index1];

        end
    else
        [maxima index1]=max(Et_say(z1,:));
        Maxima=[Maxima maxima];
        satreMaxima=[satreMaxima z1];
        Index=[Index index1];
    end


    minima1=maxima;
    minima2=maxima;
    index2=[];
    index3=[];
    for ii=1:index1-1
        if Et_say(z1,ii)>0
            if minima1>Et_say(z1,ii)
                minima1=Et_say(z1,ii);
                index2=ii;
            end
        end
    end
    index4=ii;

    for ii=index1+1:n
        if Et_say(z1,ii)>0
            if minima2>Et_say(z1,ii)
                minima2=Et_say(z1,ii);
```

```
                    index3=ii;
                end
            end
        end

        if abs(minima1-maxima)>1e-6
            Minima1=[Minima1 minima1];
            Minima11=[Minima11 minima1];
            satreMinima1=[satreMinima1 z1];
            sotooneMinima1=[sotooneMinima1 index2];
        else
              minima1=0;
              Minima11=[Minima11 minima1];
        end

        if abs(minima2-maxima)>1e-6
            Minima2=[Minima2 minima2];
            Minima22=[Minima22 minima2];
            satreMinima2=[satreMinima2 z1];
            sotooneMinima2=[sotooneMinima2 index3];
        else

              minima2=0;
              Minima22=[Minima22 minima2];
        end

end

L1X=[];
L1Y=[];
z8=0;
```

```
for z7=1:length(sotooneMinima1)
      z8=z8+1;
      l1x=XX1(satreMinima1(z8),sotooneMinima1(z7));
      L1X=[L1X l1x];
      l1y=YY1(satreMinima1(z8),sotooneMinima1(z7));
      L1Y=[L1Y l1y];

end

L2X=[];
L2Y=[];
z10=0;
for z9=1:length(sotooneMinima2)
      z10=z10+1;
      l2x=XX1(satreMinima2(z10),sotooneMinima2(z9));
      L2X=[L2X l2x];
      l2y=YY1(satreMinima2(z10),sotooneMinima2(z9));
      L2Y=[L2Y l2y];

end



L4X=[];
L4Y=[];
z13=0;

for z14=1:length(Maxima)
      z13=z13+1;
      l4x=XX1(satreMaxima(z13),Index(z14));
      L4X=[L4X l4x];
```

```
        l4y=YY1(satreMaxima(z13),Index(z14));
        L4Y=[L4Y  l4y];

end

L4X2=[];
L4Y2=[];
z132=0;

for  z14=1:length(Maxima2)
        l4x=XX1(satreMaxima2(z14),Index22(z14));
        L4X2=[L4X2  l4x];
        l4y=YY1(satreMaxima2(z14),Index22(z14));
        L4Y2=[L4Y2  l4y];
end

minima1_length=length(Minima11);
minima2_length=length(Minima22);
total_minima=Minima11+Minima22;

figure(25)
plot(L_T,total_minima)

% figure(26)
% plot(L_T(2:500),df)
% dx=L_T(2)-L_T(1);
% dE=[];
% for  i11=2:n-1
%        dU(i11)=(total_minima(i11+1)-total_minima(i11-1))/(2*dx);
%        dE=[dE dU];
% end
```

```
dx=L_T(2)-L_T(1);
dE=[];
for i11=2:n-1
      dU(i11)=(total_minima(i11+1)-total_minima(i11-1))/(2*dx);
      dE=[dE dU];
end
plot(L_T(4:end-1),dU(3:end-1))
figure(26)
mesh(XX1,YY1,Et_say)
% MyPink=pink;
% id= find(MyPink(:,1)<0.2 & MyPink(:,2)<0.2 & MyPink(:,3)<0.2);
% for i=1:size(id,1)
%       MyPink(id(i),:)=[1 1 1];
% end

% colormap(MyPink)
colormap('pink')
axis([L_T(1) L_T(n) LA(1) LA(n)])
set(gca,'XTick',[], 'YTick', [])



% figure(27)
% plot3(L1X,L1Y,Minima1,'ok')
% axis([L_T(1) L_T(n) LA(1) LA(n)])
% figure(28)
% plot3(L2X,L2Y,Minima2,'ok')
% axis([L_T(1) L_T(n) LA(1) LA(n)])
% figure(29)
% plot3(L4X(bbbb:dddd),L4Y(bbbb:dddd),Maxima(bbbb:dddd),'r')
% axis([L_T(1) L_T(n) LA(1) LA(n)])
```

```
figure(30)
% plot(L_T(2:500),df)
dx=L_T(2)-L_T(1);
dE=[];
for i11=2:n-1
    dU(i11)=(total_minima(i11+1)-total_minima(i11-1))/(2*dx);
%     dE=[dE dU];
end
hold on

plot(L_T,total_minima,'k')

legend('energy')
xlim([L_T(1) L_T(n)])
ylim([0 350])
figure(31)
plot(L_T(4:end-1),dU(3:end-1),'k')

legend('force')
axis([L_T(1) L_T(n) -2500 500])



figure(100)


hold on
plot3(XX1,YY1,Et_say)
plot3(L1X,L1Y,Minima1,'or')
plot3(L2X,L2Y,Minima2,'og')
%
```

```
bbbb=length(L4X)-sum((L4X>10.5));
dddd=sum((L4X<13));
% %
% plot3(L4X(bbbb:dddd),L4Y(bbbb:dddd),Maxima(bbbb:dddd),'oc')
plot3(L4X,L4Y,Maxima,'oc')
 axis([L_T(1) L_T(n) LA(1) LA(n)])
set(gca,'XTick',[], 'YTick', [])
```

B.2 Theoretical Analysis MATLAB Function for Cell A Compression Diode

```

function [theta_A1,theta_A2,E_A,LA_II,L_A_I_II]=CellA(LA_I,landaIa,aIa,bIa,K_A,theta0_a,n,L_o,L_c)
%
%%Designe Parameters
%Lengths
aIIa=1.25*aIa;
landaIIa=acos((aIa*cos(landaIa))/aIIa); % rigid-folding condition

%Stiffness
K1_a=2*K_A(1)*bIa;  %KIa
K2_a=2*K_A(1)*aIa;  %KIa
K3_a=2*K_A(2)*bIa;  %KIIa
K4_a=2*K_A(2)*aIIa; %KIIa
K6_a=2*L_c*K_A(3); %inter celllar crease stiffness . there are tow creases with theire associated stiffness in each unit cell
                    %Kc3_a
K7_a=8.*K_A(4).*bIa; %Kc2_a
```

```
K8_a=K_A(5).*bIa; %K_external
%Angles
phi10_a=pi-2.*theta0_a;
phi20_a=2.*asin(cos(theta0_a)./sqrt(1-((sin(theta0_a)).^2).*(sin(landaIa)).^2)); %it should not be more than 1 or -1
phi30_a=pi-(2.*acos(tan(landaIa).*(1/(tan(landaIIa))).*cos(theta0_a)));
phi40_a=2.*asin(((sin(landaIa))./(sin(landaIIa))).*sin(phi20_a./2));
phi50_a=(pi/2)+theta0_a   ;  %it should not be more than 1 or -1
s1a=sin(landaIa);
t2a=tan(landaIIa);
t1a=tan(landaIa);


%%Calculation of theta_a
theta_A1=asin(LA_I./(aIa.*sin(landaIa))); %theta angle of sheet I in new design
theta_A2=acos((cos(theta_A1).*tan(landaIa))./(tan(landaIIa))); %theta angle of sheet II in new design
LA_II=aIIa.*sin(theta_A2).*sin(landaIIa); %length of sheet II of cell A in new design
L_A_I_II=abs(aIa*s1a*((sqrt(((t2a^2)/(t1a^2))-((cos(theta_A1).^2))))-sin(theta_A1))); %total length of Cell A in new design base of original designe equation
if   (theta_A1~=0)

            phi1_a2=pi-2.*theta_A1;
            phi2_a2=2.*asin(cos(theta_A1)./sqrt(1-((sin(theta_A1)).^2).*(sin(landaIa)).^2));
            phi3_a2=pi-(2.*acos(tan(landaIa).*(1/(tan(landaIIa))).*cos(theta_A1)));
            phi4_a2=2.*asin(((sin(landaIa))./(sin(landaIIa))).*sin(phi2_a2
```

```
        ./2));
    phi5_a2=(pi/2)+theta_A1;

    E1_a2=K1_a.*(phi1_a2-phi10_a).^2;
    E2_a2=K2_a.*(phi2_a2-phi20_a).^2;
    E3_a2=K3_a.*(phi3_a2-phi30_a).^2;
    E4_a2=K4_a.*(phi4_a2-phi40_a).^2;
    E7_a2=K7_a.*(phi5_a2-phi50_a).^2;


    E_A=((E1_a2+E2_a2+E3_a2+E4_a2+E7_a2)/2);
else
    phi1_a2=0;
    phi2_a2=0;
    phi3_a2=0;
    phi4_a2=0;
    phi5_a2=0;

    E1_a2=0;
    E2_a2=0;
    E3_a2=0;
    E4_a2=0;
    E7_a2=0;
    E_A=0;

end
```

B.3 Theoretical Analysis MATLAB Function for Cell B Compression Diode

```matlab
function [E_B,LB_I_II,theta_B,E1_b2,E2_b2,E3_b2,E4_b2,E7_b2]=CellB(aIb,bIb,landaIb,LA_I,LA_II,K_B,theta0_b,L2_a_min,L2_a_max,L_A_I_II,n,LT,L_o,L_c)
% [E_B,LB_I_II,theta_B]=CellB(aIb,bIb,landaIb,LA_I,LA_II,K_B,theta0_b,L2_a_min,L2_a_max,L_A_I_II,n,LT,L_o,L_c)

%%Design Parameters
%Lengths
aIIb=1.25*aIb;
landaIIb=acos((aIb*cos(landaIb))/aIIb); % rigid-folding condition

%Stiffness
K1_b=2*K_B(1)*bIb;  %KIa
K2_b=2*K_B(1)*aIb;  %KIa
K3_b=2*K_B(2)*bIb;  %KIIa
K4_b=2*K_B(2)*aIIb; %KIIa
K6_b=2*L_c*K_B(3); %inter celllar crease stiffness . there are tow creases with theire associated stiffness in each unit cell
                   %Kc3_a
K7_b=8.*K_B(4).*bIb; %Kc2_a
K8_b=K_B(1,5).*bIb; %K_external
%Angles
s1b=sin(landaIb);
t2b=tan(landaIIb);
t1b=tan(landaIb);
A=aIb*sin(landaIb);
B=((tan(landaIIb))^2)/((tan(landaIb))^2);
theta_b=linspace(-pi/2,pi/2,n);
LB_I_II_range=aIb*s1b*((sqrt(((t2b^2)/(t1b^2))-((cos(theta_b).^2))))-sin(theta_b));
L_B_I_II_max=max(LB_I_II_range);
```

```
L_B_I_II_min=min(LB_I_II_range);
phi10_b=pi-2.*theta0_b;
phi20_b=2.*asin(cos(theta0_b)./sqrt(1-((sin(theta0_b)).^2).*(sin(landaIb)).^2)); %it should not be more than 1 or -1
phi30_b=pi-(2.*acos(tan(landaIb).*(1/(tan(landaIIb))).*cos(theta0_b)));
phi40_b=2.*asin(((sin(landaIb))./(sin(landaIIb))).*sin(phi20_b./2));
phi50_b=(pi/2)+theta0_b   ;   %it should not be more than 1 or -1


%
%           if (L_A_I_II<=L_B_I_II_max)&&(L_A_I_II>=L_B_I_II_min)
%%              if (L2_a_min<=LA_II)&&(LA_II<=L2_a_max)
%                       LB_I_II=-(LT-L_c-LA_I-L_o-L_c+LA_II);
%%                  if (L_B_I_II_max>=LB_I_II)&&(LB_I_II>=L_B_I_II_min)
%                     theta_B=real(asin((A./(2.*LB_I_II)).*(B-((LB_I_II.^2)./A^2)-1)));
%                  else
%                     theta_B=0;
%%                  end
%                     L_B2=aIIb.*sin(theta_B).*sin(landaIIb);
%%              end


          if (L2_a_min<=LA_II)&&(LA_II<=L2_a_max)
                if (L_A_I_II<=L_B_I_II_max)&&(L_A_I_II>=L_B_I_II_min)

                    LB_I_II=-(LT-L_c-LA_I-L_o-L_c+LA_II);
                if (L_B_I_II_max>=LB_I_II)&&(LB_I_II>=L_B_I_II_min)
                   theta_B=real(asin((A./(2.*LB_I_II)).*(B-((LB_I_II.^2)./A^2)-1)));
                else
```

```
                theta_B=0;
            end
                L_B2=aIIb.*sin(theta_B).*sin(landaIIb);
        end

    end
if (theta_B~=0)

        phi1_b2=pi-2.*theta_B;
        phi2_b2=2.*asin(cos(theta_B)./sqrt(1-((sin(theta_B)).^2).*(sin
            (landaIb)).^2));
        phi3_b2=pi-(2.*acos(tan(landaIb).*(1/tan(landaIIb)).*cos(
            theta_B)));
        phi4_b2=2.*asin(((sin(landaIb))./(sin(landaIIb))).*sin(phi2_b2
            ./2));
        phi5_b2=(pi/2)+theta_B;



        E1_b2=K1_b.*(phi1_b2-phi10_b).^2;
        E2_b2=K2_b.*(phi2_b2-phi20_b).^2;
        E3_b2=K3_b.*(phi3_b2-phi30_b).^2;
        E4_b2=K4_b.*(phi4_b2-phi40_b).^2;
        E7_b2=K7_b.*(phi5_b2-phi50_b).^2;
        E_B=((E1_b2+E2_b2+E3_b2+E4_b2+E7_b2)/2);
else
        phi1_b2=0;
        phi2_b2=0;
        phi3_b2=0;
        phi4_b2=0;
        phi5_b2=0;
```

```
            E1_b2=0;
            E2_b2=0;
            E3_b2=0;
            E4_b2=0;
            E7_b2=0;

            E_B=0;

end
```

B.4 Optimization analysis MATLAB Script

```

%%CELL A parameters
% a=2;
%
% b=2.8;
aIIa=1.25*a;
% landa=1.33;
landaIIa=acos((a*cos(landa))/aIIa); % rigid-folding condition
KIa=1;
K_A=zeros(1,5);
K_A(1,1)=KIa;
% Lc=
    n=5;
L_o=Lc;
```

```
theta0_a=-pi/3;


K_A(1,2)=20*KIa;
K_A(1,3)=KIa;
K_A(1,4)=KIa;
K_A(1,5)=0;
theta_a1=linspace(-pi/2,pi/2,777);
theta_a1_2=acos((cos(theta_a1).*tan(landa))./(tan(landaIIa)));
theta_a1_2_0=acos((cos(theta0_a).*tan(landa))./(tan(landaIIa)));
s1a=sin(landa);
t2a=tan(landaIIa);
t1a=tan(landa);
L1_a=a.*sin(theta_a1).*sin(landa);
L2_a=aIIa.*sin(theta_a1_2).*sin(landaIIa);
n=length(L1_a);
L2_a_max=max(L2_a);
L1_a_max=max(L1_a);
L2_a_min=min(L2_a);
L1_a_min=min(L1_a);
LA_min=L2_a_min+L1_a_min+Lc;
LA_max=L2_a_max+L1_a_max+Lc;
% LA=linspace(LA_min,LA_max,n);
LA_I=linspace(L1_a_min,L1_a_max,length(L1_a)); %length of sheet I in new
    design

%%
%%CELL B parameters
aIb=a;
bIb=aIb;
aIIb=1.25*aIb;
```

```
landaIb=landa;
landaIIb=acos((aIb*cos(landaIb))/aIIb); % rigid-folding condition
KIb=1;
K_B=zeros(1,5);
K_B(1,1)=KIb;

theta0_b=pi/3;
theta_b2_0=acos((cos(theta0_b).*tan(landaIb))./(tan(landaIIb)));

K_B(1,2)=20*KIb;
K_B(1,3)=KIb;
K_B(1,4)=KIb;
K_B(1,5)=0;
theta_b1=linspace(-pi/2,pi/2,n);
theta_b2=acos((cos(theta_b1).*tan(landaIb))./(tan(landaIIb)));
s1b=sin(landaIb);
t2b=tan(landaIIb);
t1b=tan(landaIb);
L1_b=aIb.*sin(theta_b1).*sin(landaIb);
L2_b=aIIb.*sin(theta_b2).*sin(landaIIb);
L_b=Lc+L1_b-L2_b;
L2_b_max=max(L2_b);
L1_b_max=max(L1_b);
L2_b_min=min(L2_b);
L1_b_min=min(L1_b);
%%
%Total length CEll A_I_II in  original design
A=a*sin(landa);
B=((tan(landaIIa))^2)/((tan(landa))^2);


```

```
L_a=a*s1a*((sqrt(((t2a^2)/(t1a^2))-((cos(theta_a1).^2))))-sin(theta_a1));
L_A_max=max(L_a);
L_A_min=min(L_a);
%%
%Mismatch parameters
 K_star=50;

say_A0=2*atan(cos(theta0_a)*tan(landa));
say_B0=2*atan(cos(theta0_b)*tan(landaIb));

n=length(L1_a);
%%


%%
%Calculating maximum and minium
 i5=0;
 for i3=linspace(-pi/2,pi/2,n)

     i5=i5+1;
     i6=0;
     for i4=linspace(-pi/2,pi/2,n)
         i6=i6+1;
         theta_a1_2(i5)=acos((cos(i3).*tan(landa))./(tan(landaIIa)));
         theta_b_2(i6)=acos((cos(i4).*tan(landaIb))./(tan(landaIIb)));
         total_length(i5,i6)=(Lc+(a.*sin(i3).*sin(landa))-abs((aIIa.*sin(theta_a1_2(i5)).*sin(landaIIa))))+(Lc+(aIb.*sin(i4).*sin(landaIb))-abs((aIIb.*sin(theta_b_2(i6)).*sin(landaIIb))))+L_o;
     end
```

```
end
L_total_min=min(min(total_length));
L_total_max=max(max(total_length));
L_T=linspace(L_total_min,L_total_max,n); %New design total length
%%

i1=0;
for LT=linspace(L_total_min,L_total_max,n)
      i1=i1+1;
   for i2=1:length(L1_a)
            [theta_A1(i1,i2),theta_A2(i1,i2),E_A(i1,i2),LA_II(i1,i2),
                L_A_I_II(i1,i2)]=CellA_opt(LA_I(i2),landa,a,b,K_A,theta0_a,n
                ,L_o,Lc);
            [E_B(i1,i2),LB_I_II(i1,i2),theta_B(i1,i2),E1_b2(i1,i2),E2_b2(i1,
                i2),E3_b2(i1,i2),E4_b2(i1,i2),E7_b2(i1,i2)]= CellB_opt(aIb,
                aIIb,landaIb,LA_I(i2),LA_II(i1,i2),K_B,theta0_b,L2_a_min,
                L2_a_max,L_A_I_II(i1,i2),n,LT,L_o,Lc);
            if E_B(i1,i2)~=0
                say_A(i1,i2)=2*atan((cos(theta_A1(i1,i2)))*tan(landa));
                say_B(i1,i2)=2*atan((cos(theta_B(i1,i2)))*tan(landaIb));
                E_say(i1,i2)=K_star*b*(((say_A(i1,i2)-say_B(i1,i2)).^2)./2);
                E6_a2(i1,i2)=(K_A(3).*(say_A(i1,i2)-say_A0).^2)./2;
                E6_b2(i1,i2)=(K_B(3).*(say_B(i1,i2)-say_B0).^2)./2;
                E8_A_B(i1,i2)=(K_A(5).*(say_B(i1,i2)-say_A(i1,i2)).^2)./2;

                Et_A_B(i1,i2)=E_A(i1,i2)+E_B(i1,i2);
                Et_say(i1,i2)=Et_A_B(i1,i2)+E_say(i1,i2)+E8_A_B(i1,i2)+E6_a2(
                    i1,i2)+E6_b2(i1,i2);
            else
                say_A(i1,i2)=0;
```

```
                    say_B(i1,i2)=0;
                    E_say(i1,i2)=0;
                    E6_a2(i1,i2)=0;
                    E6_b2(i1,i2)=0;
                    E8_A_B(i1,i2)=0;
                    Et_A_B(i1,i2)=0;
                    Et_say(i1,i2)=0;

               end
        end
end
%%
%zero_column of CEll A
kh=pi/4;


if abs(landa-kh)>0
zero_column_n=(n+1)/2;

lt_0column=(linspace(L_total_min,L_total_max,n))';







LA1_0column=0;
la_0column=LA1_0column;
theta_A1_0column=zeros(n,1);
theta_A1_0column(:,:)=asin(LA1_0column./(a.*sin(landa)));
```

```
theta_A2_0column=zeros(n,1);
theta_A2_0column(:,:)=acos((cos(theta_A1_0column).*tan(landa))./(tan(
    landaIIa)));
LA2_0column=aIIa.*sin(theta_A2_0column).*sin(landaIIa);




%
%%Designe Parameters
%Lengths
aIIa=1.25*a;
landaIIa=acos((a*cos(landa))/aIIa); % rigid-folding condition

%Stiffness
K1_a=2*K_A(1)*b;  %KIa
K2_a=2*K_A(1)*a;  %KIa
K3_a=2*K_A(2)*b;  %KIIa
K4_a=2*K_A(2)*aIIa; %KIIa
K6_a=2*Lc*K_A(3); %inter celllar crease stiffness . there are tow
    creases with theire associated stiffness in each unit cell
                  %Kc3_a
K7_a=8.*K_A(4).*b; %Kc2_a
K8_a=K_A(5).*b; %K_external
%Angles
phi10_a=pi-2.*theta0_a;
phi20_a=2.*asin(cos(theta0_a)./sqrt(1-((sin(theta0_a)).^2).*(sin(landa))
    .^2)); %it should not be more than 1 or -1
phi30_a=pi-(2.*acos(tan(landa).*(1/(tan(landaIIa))).*cos(theta0_a)));
phi40_a=2.*asin(((sin(landa))./(sin(landaIIa))).*sin(phi20_a./2));
phi50_a=(pi/2)+theta0_a  ;  %it should not be more than 1 or -1
```

```
phi1_a2_0column=pi-2.*theta_A1_0column;
phi2_a2_0column=2.*asin(cos(theta_A1_0column)./sqrt(1-((sin(
    theta_A1_0column)).^2).*(sin(landa)).^2));
phi3_a2_0column=pi-(2.*acos(tan(landa).*(1/(tan(landaIIa))).*cos(
    theta_A1_0column)));
phi4_a2_0column=2.*asin(((sin(landa))./(sin(landaIIa))).*sin(
    phi2_a2_0column./2));
phi5_a2_0column=(pi/2)+theta_A1_0column;

E1_a2_0column=K1_a.*(phi1_a2_0column-phi10_a).^2;
E2_a2_0column=K2_a.*(phi2_a2_0column-phi20_a).^2;
E3_a2_0column=K3_a.*(phi3_a2_0column-phi30_a).^2;
E4_a2_0column=K4_a.*(phi4_a2_0column-phi40_a).^2;
E7_a2_0column=K7_a.*(phi5_a2_0column-phi50_a).^2;


E_A_0column=((E1_a2_0column+E2_a2_0column+E3_a2_0column+E4_a2_0column+
    E7_a2_0column)/2);
E_A_constant_column=zeros(n,1);
E_A_constant_column(:,:)=E_A_0column;

Et_say_0column=[];
for i10=1:n
    if Et_say(i10,zero_column_n)~=0
      Edummy=Et_say(i10,zero_column_n)+E_A_0column(i10);
      Et_say_0column=[Et_say_0column;Edummy];
    else
      Edummy=0;
      Et_say_0column=[Et_say_0column;Edummy];
```

```
        end
end
Et_say(:,zero_column_n)=Et_say_0column;
end

%%
%
% %Plotting  results
for  i=1:n
        L1_a_2(i)=a.*sin(theta_A1(1,i)).*sin(landa);
        L2_a_2(i)=aIIa.*sin(theta_A2(1,i)).*sin(landaIIa);
       LA(i)=L1_a_2(i)+L2_a_2(i)+Lc;
end

[X1,Y1]=meshgrid(L_T,LA);
XX1=X1.';
YY1=Y1.';





%%

%Computing  enregy  derivative

Maxima=[];
Index=[];
Index2=[];
Index3=[];
Index4=[];
```

```
Minima1=[];
Minima2=[];
Minima3=[];
Minima4=[];
Index4=[];
Index5=[];
satreMinima1=[];
satreMinima2=[];
satreMinima3=[];
satreMinima4=[];
sotooneMinima1=[];
sotooneMinima2=[];
sotooneMinima3=[];
sotooneMinima4=[];
satreMaxima=[];
Maxima8=[];
satreMaxima8=[];
Index8=[];
first_false_maxima=[];

Minima11=[];
Minima22=[];


Index22=[];
satreMaxima2=[];
Maxima2=[];

n1=ceil(n*1545/1555);
n2=ceil(n*30/1555);
n3=ceil(n*995/1555);
```

```
for z1=1:n


    if z1<=4000000000
        [maxima,index1]=max(Et_say(z1,:));
        Maxima=[Maxima maxima];
        satreMaxima=[satreMaxima z1];
        Index=[Index index1];
    elseif z1<=n1
        aaaaa=sum(Et_say(z1,:)>0);
        if Et_say(z1,n)==0
            [maxima,index1]=max(Et_say(z1,floor(aaaaa*0.2):aaaaa-floor(aaaaa*0.4)));
            index1=index1+floor(aaaaa*0.2)-1;
            Maxima=[Maxima maxima];
            satreMaxima=[satreMaxima z1];
            Index=[Index index1];
        elseif Et_say(z1,1)==0
            [maxima index1]=max(Et_say(z1,n-aaaaa+floor(aaaaa*0.2):n-floor(aaaaa*0.2)));
            index1=index1+n-aaaaa+floor(aaaaa*0.2)-1;
            Maxima=[Maxima maxima];
            satreMaxima=[satreMaxima z1];
            Index=[Index index1];
        else
            [maxima index1]=max(Et_say(z1,n2:n3));
            index1=index1+n2-1
            Maxima=[Maxima maxima];
            satreMaxima=[satreMaxima z1];
            Index=[Index index1];
```

```

        end
    else
        [maxima index1]=max(Et_say(z1,:));
        Maxima=[Maxima maxima];
        satreMaxima=[satreMaxima z1];
        Index=[Index index1];
    end


    minima1=maxima;
    minima2=maxima;
    index2=[];
    index3=[];
    for ii=1:index1-1
        if Et_say(z1,ii)>0
            if minima1>Et_say(z1,ii)
                minima1=Et_say(z1,ii);
                index2=ii;
            end
        end
    end
    index4=ii;

    for ii=index1+1:n
        if Et_say(z1,ii)>0
            if minima2>Et_say(z1,ii)
                minima2=Et_say(z1,ii);
                index3=ii;
            end
        end
```

```
    end

    if abs(minima1-maxima)>1e-6
        Minima1=[Minima1 minima1];
        Minima11=[Minima11 minima1];
        satreMinima1=[satreMinima1 z1];
        sotooneMinima1=[sotooneMinima1 index2];
    else

            minima1=0;
            Minima11=[Minima11 minima1];
    end

    if abs(minima2-maxima)>1e-6
        Minima2=[Minima2 minima2];
        Minima22=[Minima22 minima2];
        satreMinima2=[satreMinima2 z1];
        sotooneMinima2=[sotooneMinima2 index3];
    else

            minima2=0;
            Minima22=[Minima22 minima2];
    end


end



minima1_length=length(Minima11);
minima2_length=length(Minima22);
```

```
total_minima=Minima11+Minima22;




dx=L_T(2)-L_T(1);
dE=[];
for i11=2:n-1
    dU(i11)=(total_minima(i11+1)-total_minima(i11-1))/(2*dx);
%       dE=[dE dU];
end

% figure(31)
% plot(L_T(4:end-1),dU(3:end-1),'k')
%
% legend('force')
% axis([L_T(1) L_T(n) -2500 500])


%%surface area
%cell a
A1_A=4*a*b*sin(landa)/2;
A2_A=4*aIIa*b*sin(landaIIa)/2;
A3_A=2*b*Lc;


%cell b

A1_B=4*aIb*bIb*sin(landaIb)/2;
A2_B=4*aIIb*bIb*sin(landaIIb)/2;
```

```
A3_B=2*b*Lc;

%connecting sheets

A4_C=2*b*Lc;

%total surface area

A_total=A1_A+A2_A+A3_A+A1_B+A2_B+A3_B+A4_C;


%%Finding Fe and Fc
nn=numel(dU);

%total surface area

        A_total=A1_A+A2_A+A3_A+A1_B+A2_B+A3_B+A4_C;


        %%Finding Fe and Fc
        myArray=dU(100:nn-20);
%         dU(1:15)=[];
%         dU(end:-1:nn-15)=[];
%         n_reduced=numel(dU)
        [Fc_max,Fc_max_index]=min(myArray);
        fe_rnage=myArray(1:Fc_max_index-20);
        Fe_max=max(fe_rnage);
        % length_portion=L_T(end)-L_T(1);
        %
        % portion=L_T(1)+0.4*length_portion;
        % idx=length(L_T)-sum(L_T>portion);
```

```
% index_fe=idx+1;
% index_fc=idx+2;
% fe_rnage=dU(3:index_fe);
% fc_range=dU(index_fe+1:end-1);
% Fe_max=max(fe_rnage);
% Fc_max=min(fc_range);
force_ratio=abs(Fc_max)/Fe_max;
```

Bibliography

[1] Nasim Baharisangari and Suyi Li. "Exploiting the asymmetric energy barrier in multi-stable origami to enable mechanical diode behavior in compression". In: *Proceedings of the ASME Design Engineering Technical Conference* 5B-2019 (2019), pp. 1–8. DOI: 10.1115/DETC2019-97420.

[2] Osama R. Bilal, André Foehr, and Chiara Daraio. "Bistable metamaterial for switching and cascading elastic vibrations". In: *Proceedings of the National Academy of Sciences* 114.18 (2017), pp. 4603–4606. ISSN: 0027-8424. DOI: 10.1073/pnas.1618314114. URL: http://www.pnas.org/lookup/doi/10.1073/pnas.1618314114.

[3] Landen Bowen et al. "DYNAMIC MODELING AND ANALYSIS OF AN ORIGAMI-INSPIRED OPTICAL". In: *Proceedings of the ASME 2016 Conference on Smart Materials, Adaptive Structures and Intelligent Systems* (2016), pp. 1–11.

[4] Kenneth C Bradley. "Mechanical Computing in Microelectromechanical Systems (MEMS), Thesis ". In: (2003).

[5] K N Chappanda et al. "A single nano cantilever as a reprogrammable universal logic gate". In: *Journal of Micromechanics and Microengineering* (2017), aa5dfa. ISSN: 0960-1317. DOI: 10.1088/1361-6439/aa5dfa. URL: https://doi.org/10.1088/1361-6439/aa5dfa.

[6] F. K. Chowdhury. "Micro-electro-mechanical-systems-based single- device digital logic gates for harsh environment applications". PhD thesis. 2013. URL: http://ir.obihiro.ac.jp/dspace/handle/10322/3933.

[7] Mohammed F. Daqaq et al. "On the Role of Nonlinearities in Vibratory Energy Harvesting: A Critical Review and Discussion". In: *Applied Mechanics Reviews* 66.4 (2014), p. 040801. ISSN: 0003-6900. DOI: 10.1115/1.4026278. URL: http://appliedmechanicsreviews.asmedigitalcollection.asme.org/article.aspx?doi=10.1115/1.4026278.

[8] Levi H Dudte et al. "Programming curvature using tessellations". In: *nature materials* January (2016). DOI: 10.1038/NMAT4540.

[9] Hongbin Fang, K. W. Wang, and Suyi Li. "Asymmetric energy barrier and mechanical diode effect from folding multi-stable stacked-origami". In: *Extreme Mechanics Letters* 17 (2017), pp. 7–15. ISSN: 23524316. DOI: 10.1016/j.eml.2017.09.008. URL: https://doi.org/10.1016/j.eml.2017.09.008.

[10] E T Filipov, G H Paulino, and T Tachi. "Origami tubes with reconfigurable polygonal Subject Areas :" in: *Proc Math Phys Eng Sci.* (2016).

[11] Michael P Frank, Thomas F Knight Jr, and Programable Multistable Mechanisms. "Two types of mechanical reversible logic". In: *Nanotechnology* (1993).

[12] Tobias Frenzel et al. "Tailored Buckling Microlattices as Reusable Light-Weight Shock Absorbers". In: *Advanced Materials* (2016), pp. 5865–5870. ISSN: 15214095. DOI: 10.1002/adma.201600610. arXiv: 1207.1956.

[13] Andrew Gillman et al. "Design of Soft Origami Mechanisms with Targeted Symmetries". In: *Actuators* (2018), pp. 1–16. DOI: 10.3390/act8010003.

[14] E Hawkes et al. "Programmable matter by folding". In: *PNAS* 107.28 (2010). DOI: 10.1073/pnas.0914069107.

[15] Sachiko Ishida, Taketoshi Nojima, and Ichiro Hagiwara. "Regular Folding Pattern Generation for Deployable Non-Axisymmetric Tubes". In: *Proceedings of the ASME 2014 International Design Engineering Technical Conferences Computers and Information in Engineering Conference* (2014), pp. 1–7.

[16] Cai Jianguo et al. "Bistable Behavior of the Cylindrical Origami Structure With Kresling Pattern". In: *Journal of Mechanical Design* 137.June (2015), pp. 1–8. DOI: 10.1115/1.4030158.

[17] Meredith Johnson et al. "Fabricating biomedical origami : a state-of-the-art review". In: *International Journal of Computer Assisted Radiology and Surgery* (2017), pp. 2023–2032. DOI: 10.1007/s11548-017-1545-1.

[18] Kaori Kuribayashi et al. "Self-deployable origami stent grafts as a biomedical application of Ni-rich TiNi shape memory alloy foil". In: *Materials Science Engineering* 419 (2006), pp. 131–137. DOI: 10.1016/j.msea.2005.12.016.

[19] Rolf Landauer. "Dissipation ans noise immunity in computation and communication". In: *nature* i (1988), pp. 3–8.

[20] Robert J Lang, Spencer Magleby, and Larry Howell. "Single Degree-of-Freedom Rigidly Foldable Cut Origami Flashers". In: *Journal of Mechanisms and Robotics* 8.June (2016), pp. 1–15. DOI: 10.1115/1.4032102.

[21] Robert J Lang et al. "Thick Rigidly Foldable Origami Mechanisms Based on Synchronized Offset Rolling Contact Elements". In: *Journal of Mechanisms and Robotics* 9.April (2017). DOI: 10.1115/1.4035686.

[22] Arthur Lebée. "From Folds to Structures , a Review". In: *International Journal of Space Structure* 30.June 2015 (2015). DOI: 10.1260/0266-3511.30.2.55.

[23] Suyi Li and K. W. Wang. “Fluidic origami with embedded pressure dependent multi-stability: A plant inspired innovation”. In: *Journal of the Royal Society Interface* 12.111 (2015). ISSN: 17425662. DOI: 10.1098/rsif.2015.0639.

[24] Suyi Li et al. “Architected Origami Materials : How Folding Creates Sophisticated Mechanical Properties”. In: *Advanced Materials* 1805282 (2019), pp. 1–18. DOI: 10.1002/adma.201805282.

[25] Alexander E Marras et al. “Programmable motion of DNA origami mechanisms”. In: *PNAS* 112.3 (2015), pp. 713–718. DOI: 10.1073/pnas.1408869112.

[26] Pierre-olivier Mouthuy et al. “of rings from curved origami to foldable tents”. In: *Nature Communications* (2012). DOI: 10.1038/ncomms2311.

[27] Yutaka Nishiyama. “Miura folding: Applying origami to space exploration”. In: April (2012).

[28] Young Seok Oh. “Synthesis of Multistable Equilibrium Compliant Mechanisms Using Combinations of Bistable Mechanisms”. In: *Journal of Mechanical Design* 131.February (2009), pp. 1–11. DOI: 10.1115/1.3013316.

[29] Jamie Paik. “Robogami : A Fully Integrated Low-Profile Robotic Origami”. In: *Journal of Mechanisms and Robotics* 7.May (2015), pp. 1–8. DOI: 10.1115/1.4029491.

[30] Sergio Pellegrino. “Manufacture of Arbitrary Cross-Section Composite Honeycomb Cores Based on Origami Techniques”. In: *Journal of Mechanical Design* (2014). DOI: 10.1115/1.4026824.

[31] Rui Peng. “Origami of thick panels”. In: *SCIENCE* July (2015). DOI: 10.1126/science.aab2870.

[32] K. W. Wang R. L. Harne. “A review of the recent research on vibration energy harvesting via bistable systems”. In: *Smart Materials and Structures* (2013). DOI: 10.1088/0964-1726/22/2/023001.

[33] K. W. Wang R. L. Harne Z. Wu. “Designing and Harnessing the Metastable States of a Modular Metastructure for Programmable Mechanical Properties Adaptation”. In: *Journal of Mechanical Design* 138.February (2016), pp. 1–9. DOI: 10.1115/1.4032093.

[34] Jordan R Raney et al. “Stable propagation of mechanical signals in soft media using stored elastic energy”. In: *PNAS* 113.35 (2016). DOI: 10.1073/pnas.1604838113.

[35] John Rogers et al. “Origami MEMS and NEMS”. In: *MRSBulletin* May (2016), pp. 123–129. DOI: 10.1557/mrs.2016.2.

[36] M. L. Roukes. “Mechanical compution, redux?” In: *Technical Digest - International Electron Devices Meeting, IEDM* (2004), pp. 539–542. ISSN: 01631918. DOI: 10.1109/iedm.2004.1419213.

[37] Pole S. “MOGA-II - An improved Multi-Objective Genetic Algorithm.” In: *Technical Report* (2003-006).

[38] Mark Schenk and Simon D. Guest. “Geometry of Miura-folded metamaterials”. In: *Proceedings of the National Academy of Sciences* 110.9 (2013), pp. 3276–3281. ISSN: 0027-8424. DOI: 10.1073/pnas.1217998110. URL: http://www.pnas.org/lookup/doi/10.1073/pnas.1217998110.

[39] Mark Schenk et al. “Review of Inflatable Booms for Deployable Space Structures : Packing and Rigidization”. In: *Journal of Spacecraft and Rockets* 51.3 (2014), pp. 762–778. DOI: 10.2514/1.A32598.

[40] Yuanping Song et al. “Additively manufacturable micro-mechanical logic gates”. In: *Nature Communications* 2019 (), pp. 1–6. ISSN: 2041-1723. DOI: 10.1038/s41467-019-08678-0. URL: http://dx.doi.org/10.1038/s41467-019-08678-0.

[41] Tomohiro Tachi. “Composite Rigid-Foldable Curved Origami Structure”. In: *Proceedings of the First Conference Transformables* 1 (2013), pp. 1–6.

[42] Benjamin Treml et al. “Origami mechanologic”. In: *PNAS* 0 (2018). DOI: 10.1073/pnas.1805122115.

[43] Patsy Wang-iverson and Robert J Lang. *Fifth International Meeting of Origami Science, Mathematics, and Education*. ISBN: 9781439873502.

[44] H Yasuda et al. “Reentrant Origami-Based Metamaterials with Negative Poisson ’ s Ratio and Bistability”. In: *Physical Review Letters* May (2015). DOI: 10.1103/PhysRevLett.114.185502.

[45] Shannon A Zirbel et al. “Accommodating Thickness in Origami-Based Deployable”. In: *Journal of Mechanical Design* 135.November (2013), pp. 1–11. DOI: 10.1115/1.4025372.